https://ntrs.nasa.gov/search.jsp?R=19920001847 2017-08-15T21:38:04+00:00Z

NASA Contractor Report 4409

Prediction of the Pattern Performance for the Aeroassist Flight Experiment (AFE) Spacecraft

C. Yang, R. Rudduck,
and R. Torres
The Ohio State University
ElectroScience Laboratory
Columbus, Ohio

Prepared for
Langley Research Center
under Contract NAS1-17450

National Aeronautics and
Space Administration

Office of Management

Scientific and Technical
Information Program

1991

INTENTIONALLY BLANK

Contents

List of Figures iv

1 Introduction 1

2 Free Space Patterns 4

2.1 Spacecraft 4

2.2 Antenna modeling 5

3 AFE with Re-entry Plasma 13

3.1 Introduction 13

3.2 Free space patterns 13

3.3 Patterns with re-entry plasma 14

3.3.1 Antenna Location 1 14

3.3.2 Antenna Location 2 18

3.3.3 Antenna Location 3 18

4 Summary and Conclusions 38

References 40

Appendix A Input and Output Files of the OSU Aircraft Antenna Code 41

Appendix B Input and Output Files of the Ray Tracing Program 44

PRECEDING PAGE BLANK NOT FILMED

List of Figures

1.1 Deployment of the AFE spacecraft by the Space Shuttle. . . 2

1.2 Communications links between the AFE spacecraft and the TDRS satellites during the Aeropass data period. 3

2.1 Typical antenna location on the AFE spacecraft 5

2.2 Definition of ellipsoid geometry. 7

2.3 Micropatch antenna. (a) Geometry (b) Equivalent magnetic loop source. 8

2.4 E-plane free space patterns in the xz plane for E-polarization in the xz plane. Solid Line : measured from NASA Langley ; Dotted Line : calculated from OSU Aircraft Antenna Code. 9

2.5 H-plane free space patterns in the transverse plane for E-polarization in the xz plane. Solid Line : measured from NASA Langley ; Dotted Line : calculated from OSU Aircraft Antenna Code. 10

2.6 H-plane free space patterns in the xz plane for E-polarization in the transverse plane. Solid Line : measured from NASA Langley ; Dotted Line : calculated from OSU Aircraft Antenna Code. 11

2.7 E-plane free space patterns in the transverse plane for E-polarization in the transverse plane. Solid Line : measured from NASA Langley ; Dotted Line : calculated from OSU Aircraft Antenna Code. 12

3.1 E-plane free space pattern of the micropatch antenna on an infinite ground plane. 15

3.2 H-plane free space pattern of the micropatch antenna on an infinite ground plane. 16

3.3 AFE re-entry plasma sheath densities. 17

3.4 The multiple wedge-shaped layers used to simulate the AFE re-entry plasma around Antenna Location 1. 20

3.5 Comparison of the H-plane patterns for Antenna Location 1 radiating into plasma and free space. The electron densities of the contour lines are lowered with the values shown, and the collision frequency is zero. 21

3.6 Comparison of the 45°-plane patterns for Antenna Location 1 radiating into plasma and free space. The electron densities of the contour lines are lowered with the values shown, and the collision frequency is zero. 22

3.7 Comparison of the E-plane patterns for Antenna Location 1 radiating into plasma and free space. The electron densities of the contour lines are lowered with the values shown, and the collision frequency is zero. 23

3.8 Comparison of the H-plane patterns for Antenna Location 1 radiating into plasma and free space for various collision frequencies. The electron densities of the contour lines are divided by $10^{3.5}$. 24

3.9 Comparison of the 45°-plane patterns for Antenna Location 1 radiating into plasma and free space for various collision frequencies. The electron densities of the contour lines are divided by $10^{3.5}$. 25

3.10 Comparison of the E-plane patterns for Antenna Location 1 radiating into plasma and free space for various collision frequencies. The electron densities of the contour lines are divided by $10^{3.5}$. 26

3.11 The multiple wedge-shaped layers used to simulate the AFE re-entry plasma around Antenna Location 2. 27

3.12 Comparison of the H-plane patterns for Antenna Location 2 radiating into plasma and free space. The electron densities of the contour lines are lowered with the values shown, and the collision frequency is zero. 28

3.13 Comparison of the 45°-plane patterns for Antenna Location 2 radiating into plasma and free space. The electron densities of the contour lines are lowered with the values shown, and the collision frequency is zero. 29

3.14 Comparison of the E-plane patterns for Antenna Location 2 radiating into plasma and free space. The electron densities of the contour lines are lowered with the values shown, and the collision frequency is zero. 30

3.15 Comparison of the H-plane patterns for Antenna Location 2 radiating into plasma and free space for various collision frequencies. The electron densities of the contour lines are divided by 10^3. 31

3.16 Comparison of the 45°-plane patterns for Antenna Location 2 radiating into plasma and free space for various collision frequencies. The electron densities of the contour lines are divided by 10^3. 32

3.17 Comparison of the E-plane patterns for Antenna Location 2 radiating into plasma and free space for various collision frequencies. The electron densities of the contour lines are divided by 10^3. 33

3.18 The multiple wedge-shaped layers used to simulate the AFE re-entry plasma around Antenna Location 3. 34

3.19 Comparison of the H-plane patterns for Antenna Location 3 radiating into plasma and free space. The electron densities of the contour lines are lowered with the values shown, and the collision frequency is zero. 35

3.20 Comparison of the H-plane patterns for Antenna Location 3 radiating into plasma and free space for various collision frequencies. The electron densities of the contour lines are divided by $10^{1.7}$. 36

3.21 Comparison of the H-plane patterns for Antenna Location 3 radiating into plasma and free space for various collision frequencies. The electron densities of the contour lines are divided by $10^{1.5}$. 37

Chapter 1

Introduction

A series of recent studies [1]-[3] have focused attention on a class of missions in which a reusable Aeroassisted Orbit Transfer Vehicle (AOTV) would be used for the delivery and return of cargo, servicing equipment and personnel between low and high Earth orbit (or the Moon). On return from high orbit, these vehicles typically enter the outer fringes of the Earth's atmosphere with a velocity of approximately 34,000 ft/sec, fly a roll-modulated trajectory with a perigee of 250,000 to 300,000-ft altitude, skip back out of the atmosphere, and rendezvous with a Space Station after having achieved the velocity decrement (9,000 ft/sec) required for capture into low Earth orbit.

In order to provide a set of benchmark flight data that could be used to validate computational fluid dynamics analysis and allow optimum engineering design of such vehicles, the National Aeronautics and Space Administration has undertaken the Aeroassist Flight Experiment (AFE). The AFE spacecraft, sub-scale vehicle of the AOTV, will be launched from the Space Shuttle as depicted in Figure 1.1. The AFE spacecraft will fly a representative aeroassist trajectory and then record sensor measurements of aerodynamic performance, thermal protection response, and plasma-ionization effects during entry. After the completion of the aerospace data period, the AFE spacecraft will be recovered by the Shuttle for post flight examination

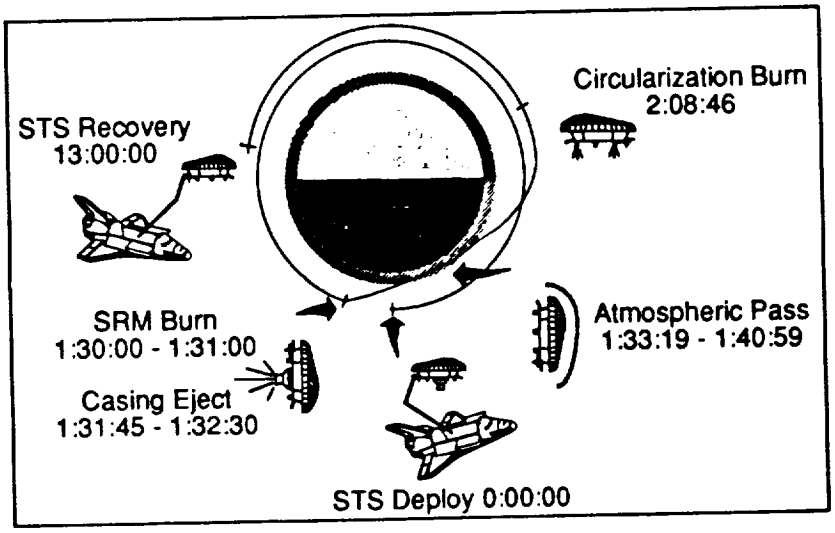

Figure 1.1: Deployment of the AFE spacecraft by the Space Shuttle.

and analysis.

The research reported here concerns the spacecraft antennas for AFE in order to provide estimates for signal transmissions from AFE to the Tracking and Data Relay Satellites (TDRS) during the aeropass data period. The AFE-TDRS communications links are shown in Figure 1.2 and these telecommunications links are vital to the success of the AFE mission.

This report describes the computer modeling of the antennas on the spacecraft with and without the re-entry plasma. The free space patterns for the antenna on the AFE vehicle were calculated by applying the Ohio State University Aircraft Antenna Code [4]. In Chapter 2, the calculated free space patterns are compared to the patterns measured at NASA Langley for a 0.4 scale model of the AFE vehicle. Then, in Chapter 3 the radiation patterns in the presence of the plasma layers evaluated from the Ray-Tracing Approach [5] are predicted based on estimated profiles.

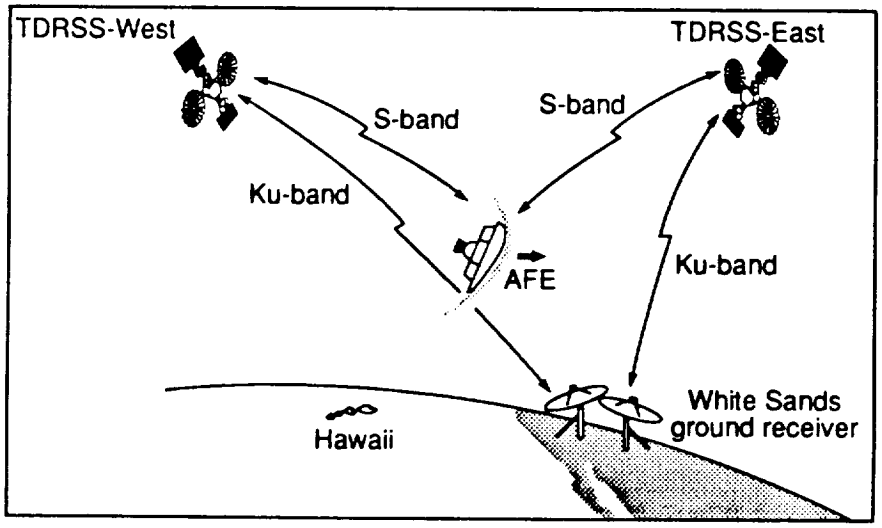

Figure 1.2: Communications links between the AFE spacecraft and the TDRS satellites during the Aeropass data period.

Chapter 2

Free Space Patterns

2.1 Spacecraft

A profile view of the AFE spacecraft is shown in Figure 2.1. Various antenna locations are being considered to provide adequate coverage for the communications link between the spacecraft and the TDRS satellites. Free space pattern measurements were obtained from a 0.4 scale model of the AFE vehicle fabricated for NASA Langley. The antenna location for which patterns were measured is shown in Figure 2.1.

The scaled spacecraft was modeled by an ellipsoid in The Ohio State University Aircraft Code [4]. This code uses the Geometrical Theory of Diffraction as its basic modeling technique. The geometry parameters of the ellipsoid were chosen to model the spacecraft surface as closely as possible near the antenna aperture.

The parameters used to describe the composite ellipsoid are shown in Figure 2.2. The values used for this case are as follows:

$$AX = 40 \tag{2.1}$$

$$BX = 72 \tag{2.2}$$

$$CX = 100 \tag{2.3}$$

$$DX = 52. \tag{2.4}$$

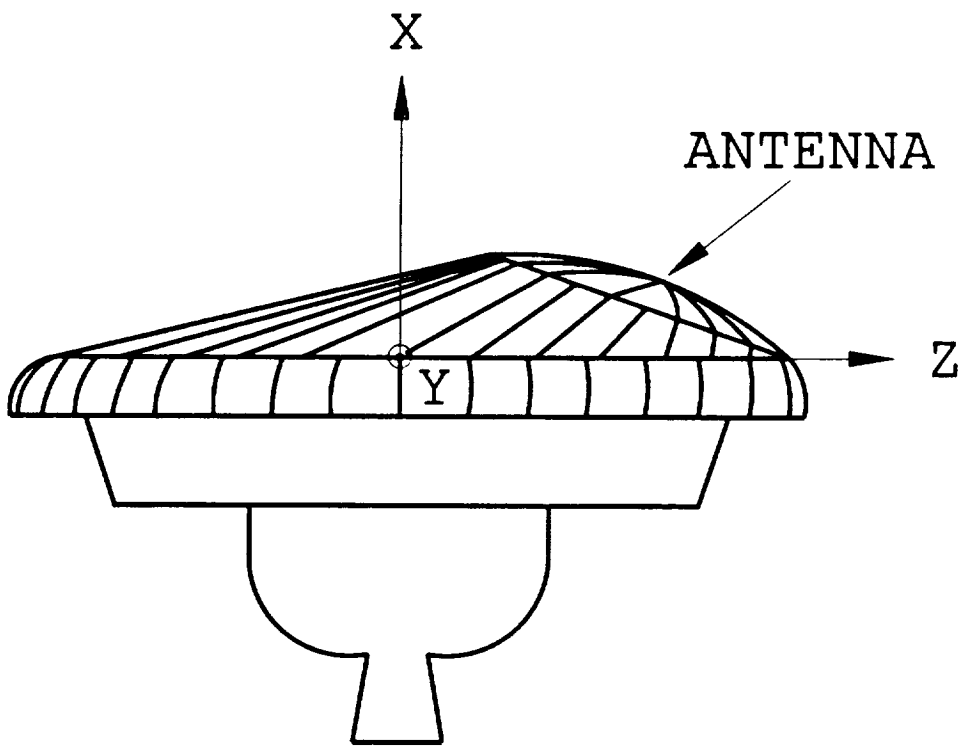

Figure 2.1: Typical antenna location on the AFE spacecraft

All values are in inches. Since the Aircraft Code does not have the capability to model half an ellipsoid, the bottom section of the spacecraft was replaced with an elliptical surface. The modeling of the spacecraft by a full ellipsoid provides good results for the forward hemisphere of the pattern coverage. This model still provides a reasonable estimate of the rear hemisphere coverage, where the pattern levels are probably too small for use in the AFE-TDRS communications links.

2.2 Antenna modeling

The antenna (0.4 scale model) used in the pattern measurement was a 0.85-inch diameter circular micropatch antenna flush mounted to the spacecraft as shown in Figure 2.3(a). The micropatch antenna was modeled using the

cavity model of Lo, et al [6] which consists of a magnetic current around the circumference of the patch. The (1,1) circular cavity mode is appropriate for our micropatch antenna, because the antenna frequency is near the resonant frequency of the (1, 1) mode. Consequently, the equivalent source is a circular loop of circumferentially-directed magnetic current with a distribution given by

$$\vec{M} = \hat{\phi}\cos(\phi) \tag{2.5}$$

as shown in Figure 2.3(b). A total of twelve magnetic current elements were used to represent the magnetic current loop in the Aircraft Code.

The measured and calculated free space patterns were obtained at 5.4 GHz for the antenna mounted at the location shown in Figure 2.1. The pattern comparisons are shown in Figures 2.4 and 2.5 for the case where the E-field polarization is in the x-z plane. As can be seen from these figures, the computer model provides good results for the entire H-plane pattern and the forward half of the E-plane pattern. As previously noted, the rear half of the pattern coverage is probably too low for the AFE-TDRS communications links.

The pattern comparison for the E-field antenna polarization in the transverse plane (E perpendicular to the x-z plane) are shown in Figures 2.7 and 2.6. In this case, the computer model provides excellent results for the forward half of the pattern coverage, and reasonable results for the rear half.

The input data file used for the Aircraft Antenna Code is listed in Appendix A for the pattern in Figure 2.4. An output data file is also listed in Appendix A which gives some sample pattern data.

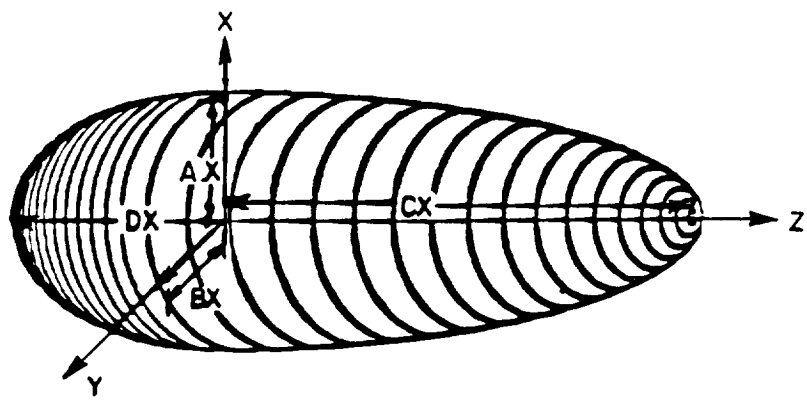

Figure 2.2: Definition of ellipsoid geometry.

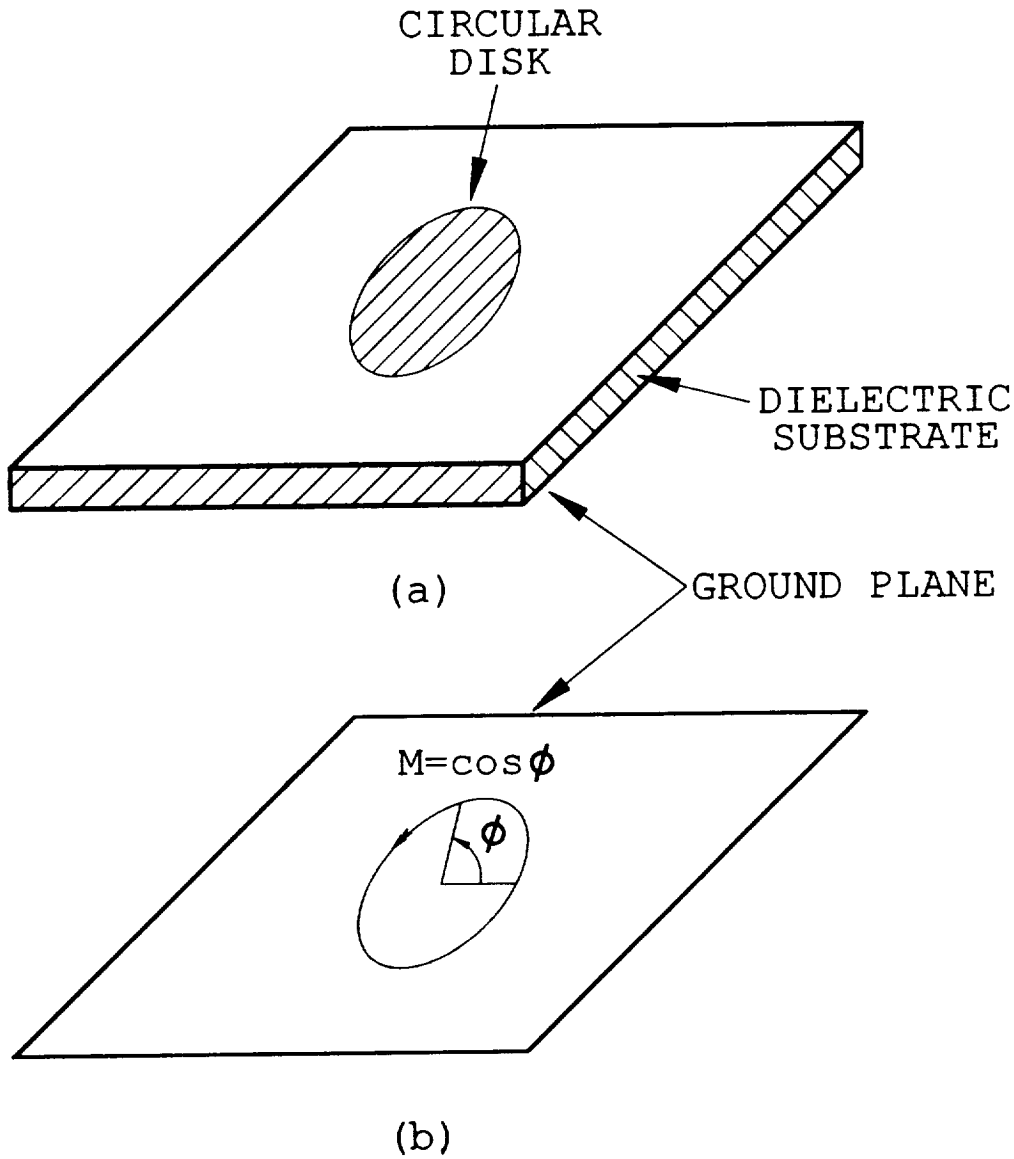

Figure 2.3: Micropatch antenna. (a) Geometry (b) Equivalent magnetic loop source.

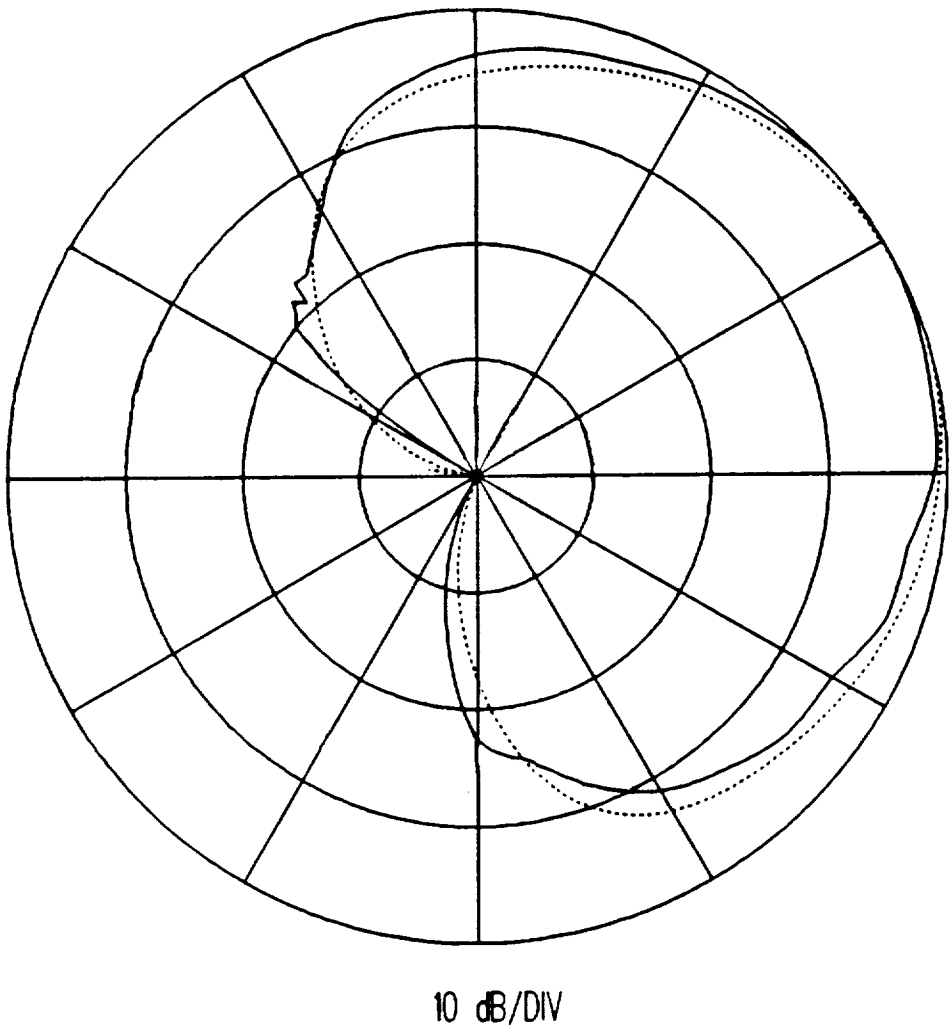

Figure 2.4: E-plane free space patterns in the xz plane for E-polarization in the xz plane. Solid Line : measured from NASA Langley ; Dotted Line : calculated from OSU Aircraft Antenna Code.

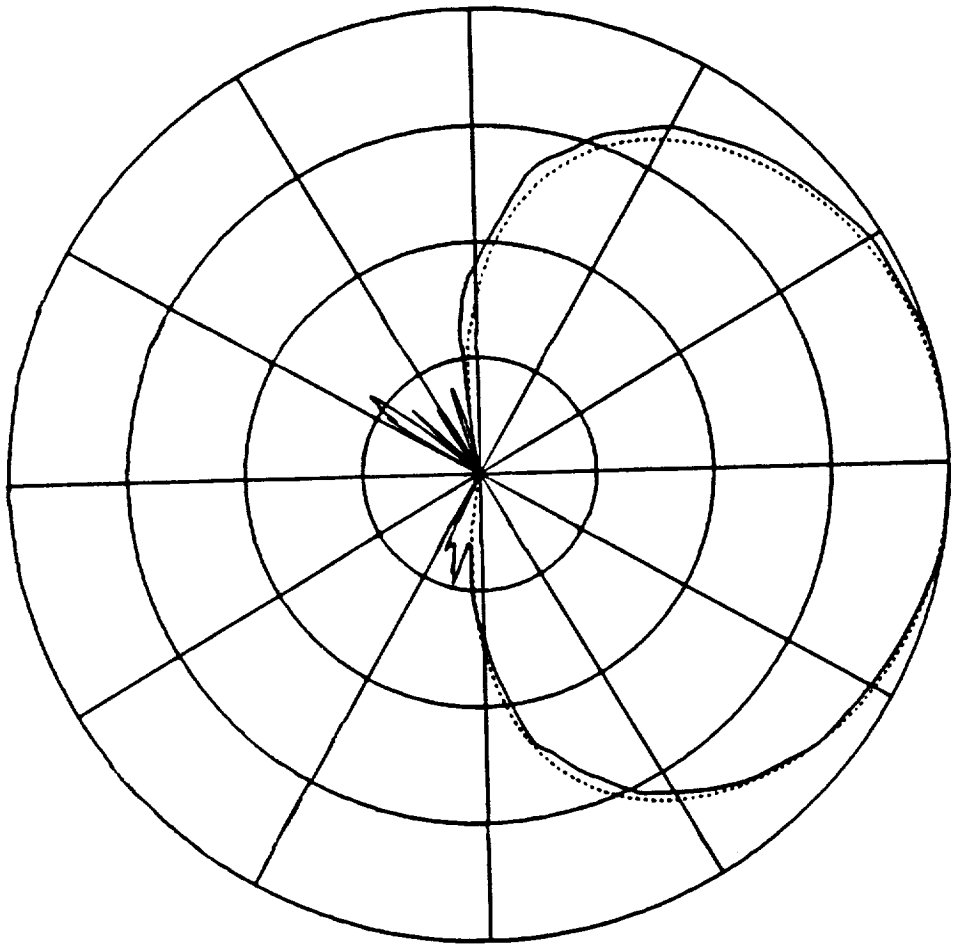

Figure 2.5: H-plane free space patterns in the transverse plane for E-polarization in the xz plane. Solid Line : measured from NASA Langley ; Dotted Line : calculated from OSU Aircraft Antenna Code.

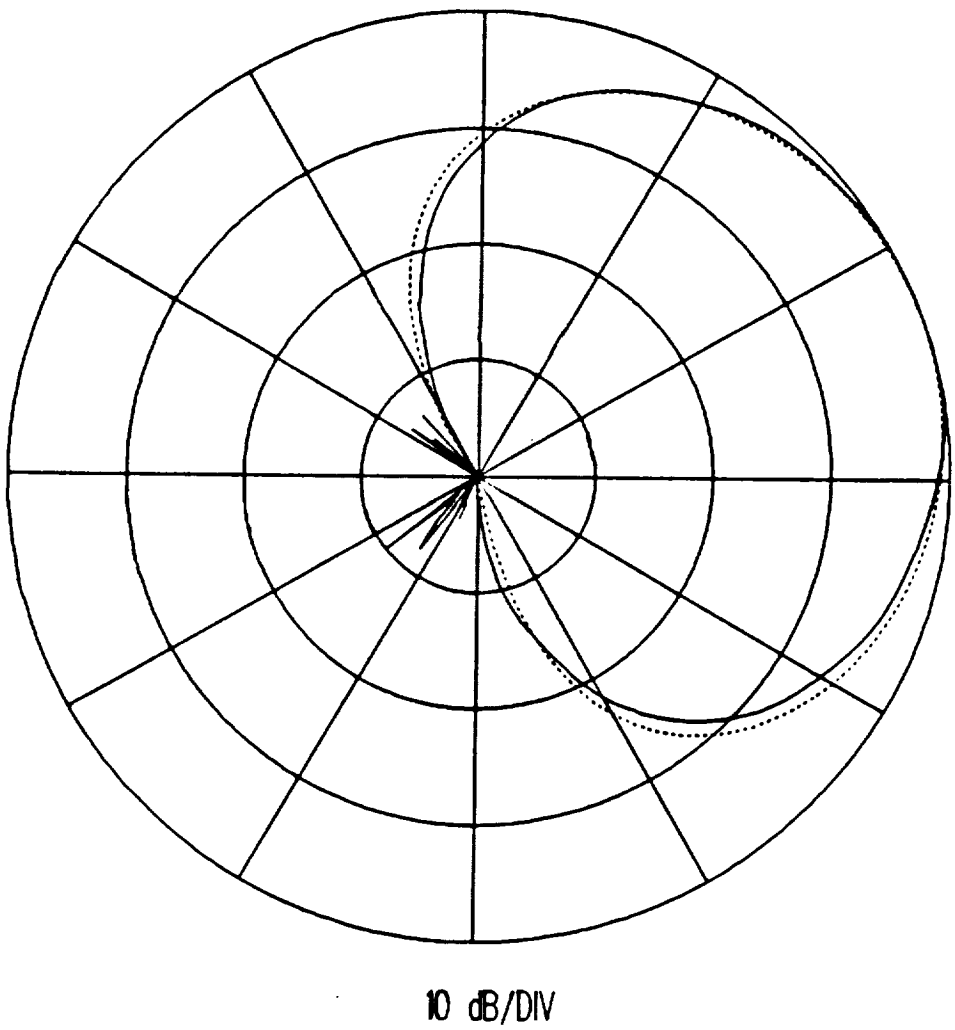

Figure 2.6: H-plane free space patterns in the xz plane for E-polarization in the transverse plane. Solid Line : measured from NASA Langley ; Dotted Line : calculated from OSU Aircraft Antenna Code.

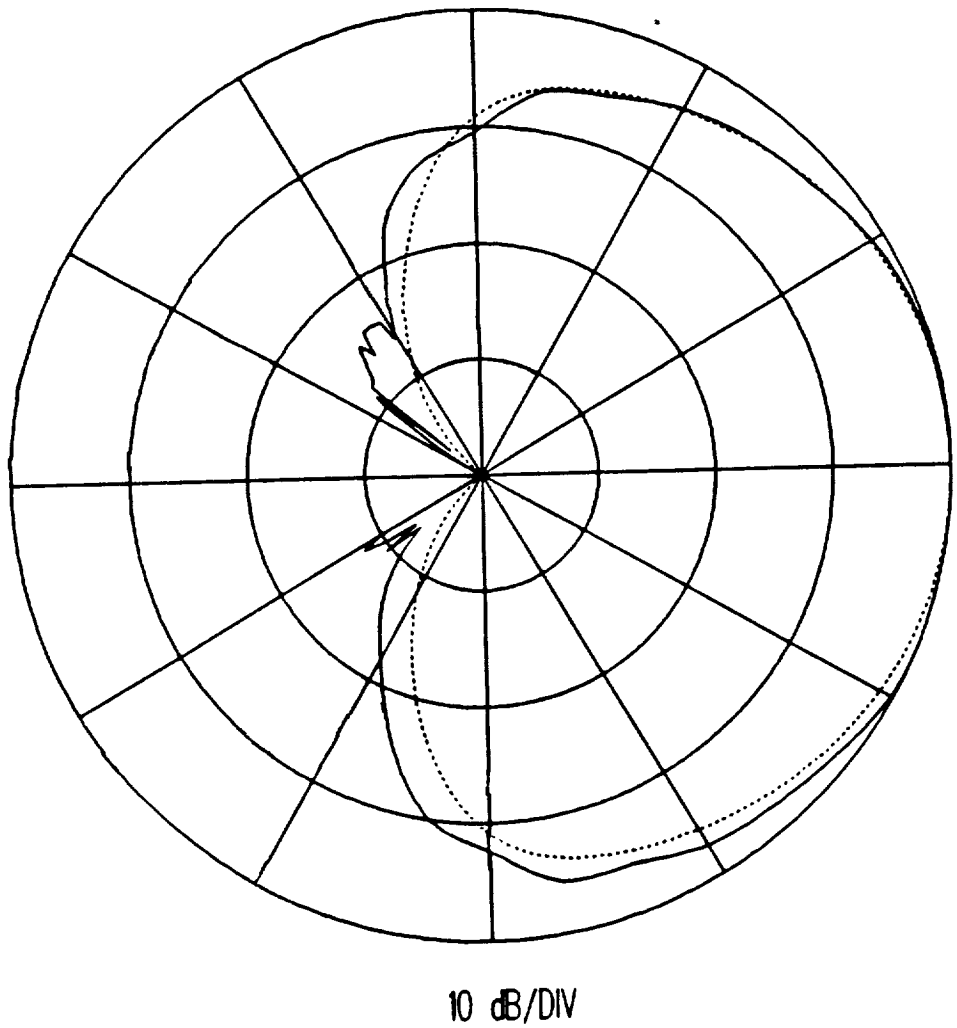

Figure 2.7: E-plane free space patterns in the transverse plane for E-polarization in the transverse plane. Solid Line : measured from NASA Langley ; Dotted Line : calculated from OSU Aircraft Antenna Code.

Chapter 3

AFE with Re-entry Plasma

3.1 Introduction

In this chapter, some radiation pattern predictions are made for the AFE antennas with the effect of the re-entry plasma at a frequency of 2.26 GHz (true scale model). These patterns were calculated from our computer code for an aperture antenna radiating into plasma layers with wedge shapes [5]. This code uses the ray tracing approach because of the wedge shapes of the plasma layers. The antenna modeled was a 2-inch diameter circular micropatch antenna and the surface of the AFE vehicle was replaced with an infinite ground plane tangential to the antenna. The radiation from the circular micropatch antenna was approximated with that from a circular loop of circumferentially-directed magnetic current as shown in Equation (2.5).

3.2 Free space patterns

The calculated free space patterns of the micropatch antenna on an infinite ground plane are shown in Figures 3.1 and 3.2 for E and H plane solutions respectively. Comparing these two results with those calculated from the OSU Aircraft Code, one observes that reasonable agreement is obtained for the forward half of the patterns even for angles close to the ground plane.

This suggests that the ground plane model for the AFE vehicle with the re-entry plasma should be accurate enough for the forward hemisphere of coverage.

3.3 Patterns with re-entry plasma

An example of the re-entry plasma profile around the AFE vehicle is plotted in Figure 3.3. The radiation patterns were calculated for three antenna locations on the vehicle as shown in Figure 3.3. The results are given in the following three subsections. The plasma layers are modeled with dielectric layers whose complex dielectric constants are given by [5]

$$\epsilon = \epsilon' - j\epsilon'' \tag{3.1}$$

where

$$\epsilon' = \epsilon_o(1 - \frac{1}{(\omega/\omega_p)^2 + (\nu/\omega_p)^2}) \tag{3.2}$$

$$\epsilon'' = \epsilon_o(\frac{\nu/\omega}{(\omega/\omega_p)^2 + (\nu/\omega_p)^2}) \tag{3.3}$$

and

$$\omega_p = \frac{Nq^2}{m\epsilon_o}, \text{the plasma frequency} \tag{3.4}$$

in which ω is the antenna frequency, ν is the collision frequency, N is the electron density, q is the electron charge, m is the electron mass, and ϵ_o is the permittivity of free space. Since the suggested plasma densities were over dense, we calculated several examples in which the plasma densities were reduced.

3.3.1 Antenna Location 1

The plasma layers which simulate the plasma profile near Antenna Location 1 are shown in Figure 3.4. Smooth variations in the plasma density were

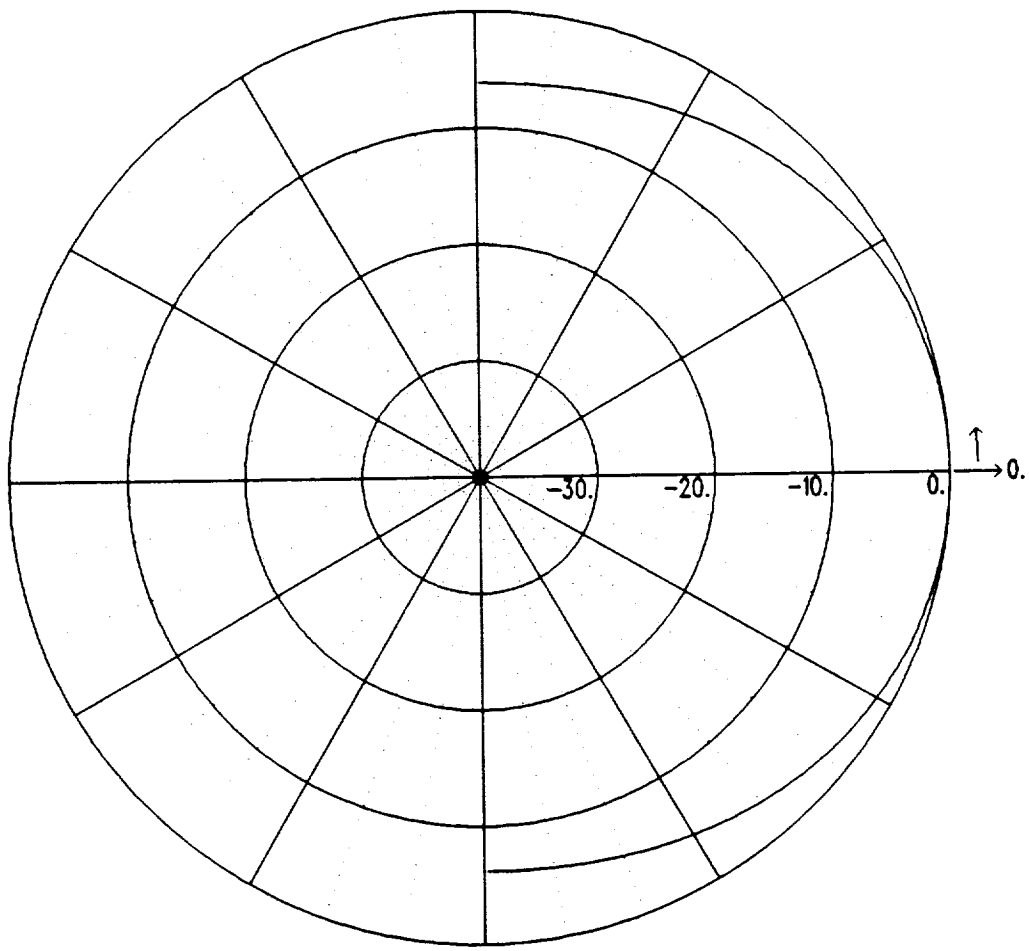

Figure 3.1: E-plane free space pattern of the micropatch antenna on an infinite ground plane.

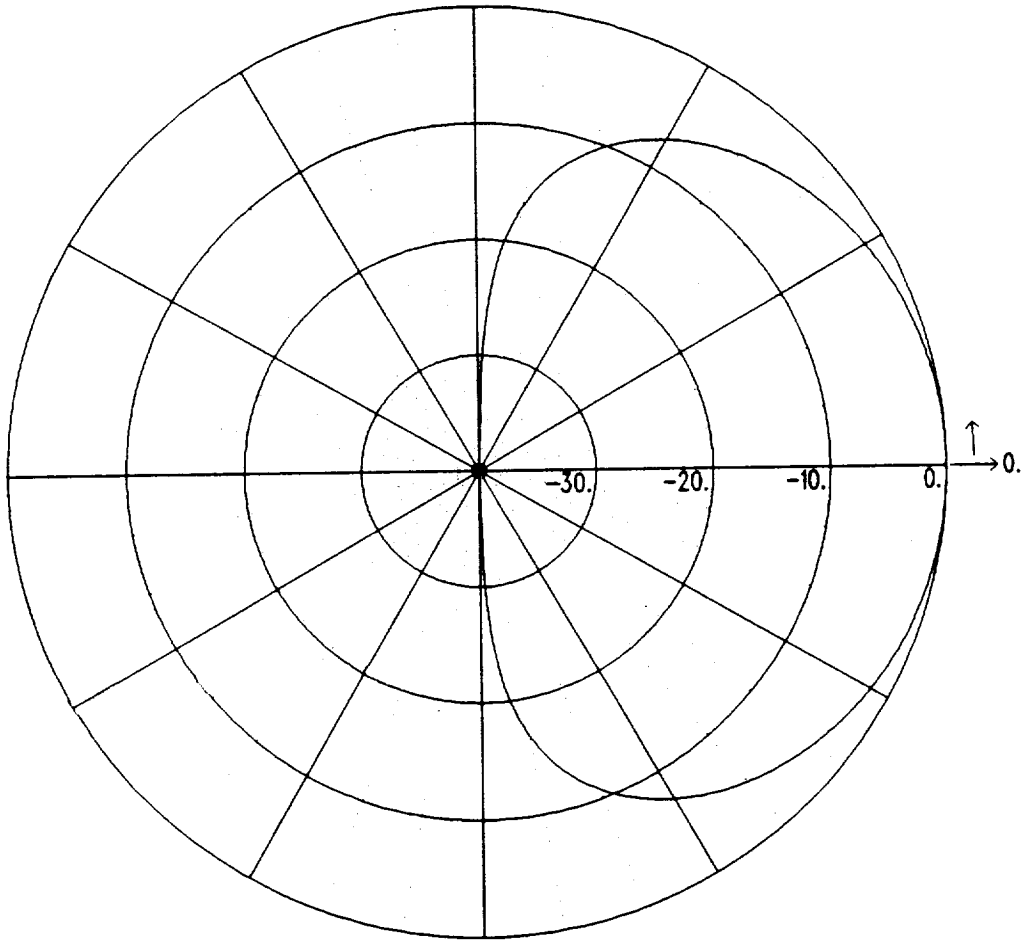

Figure 3.2: H-plane free space pattern of the micropatch antenna on an infinite ground plane.

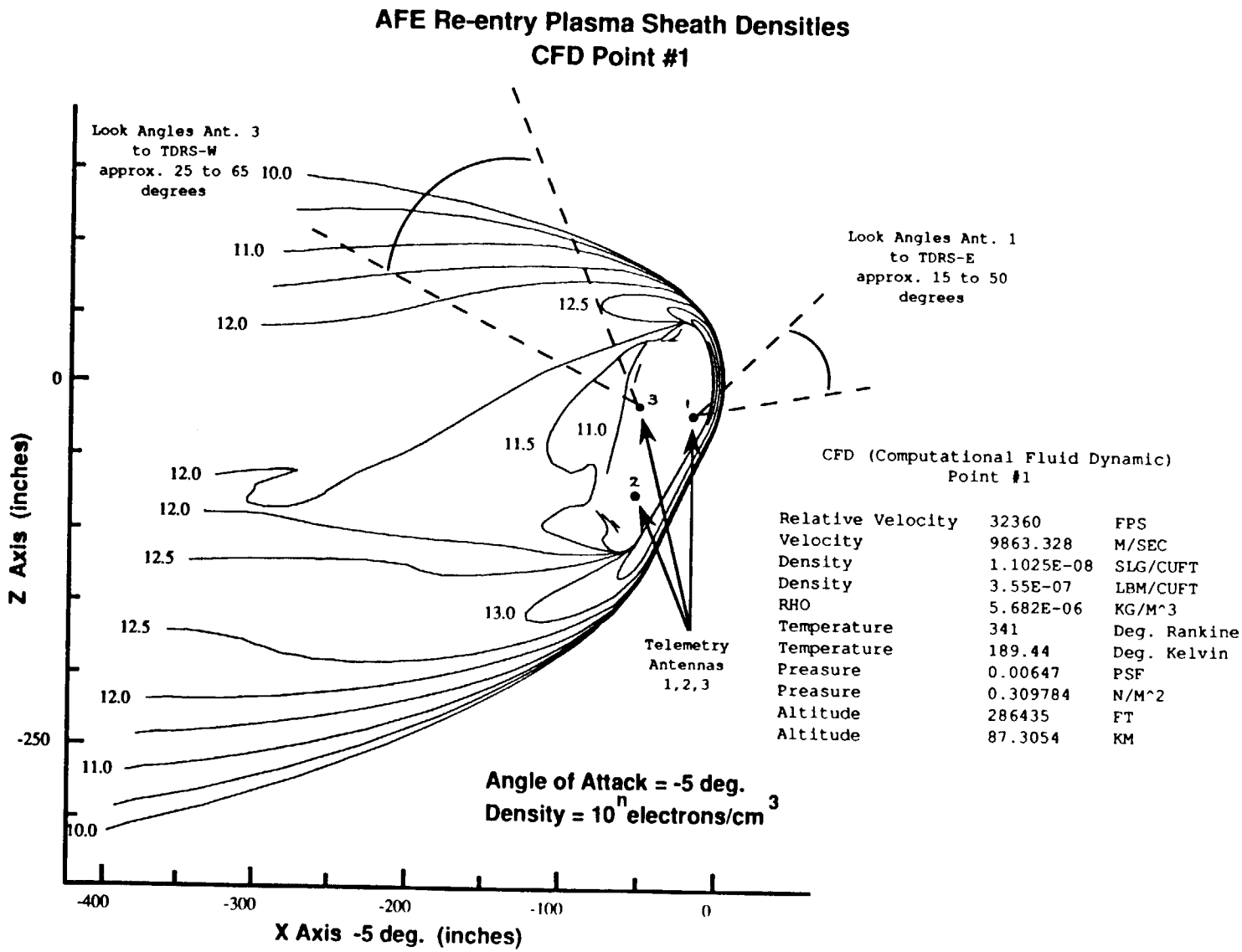

Figure 3.3: AFE re-entry plasma sheath densities.

achieved by using numerous wedge-shaped layers. The radiation patterns along the H, 45°, and E planes ($\overline{M} = \sin\phi$) are shown in Figures 3.5-3.7 together with the free space patterns for several different levels of electron densities without considering plasma losses (collision frequency $\nu = 0$). In Figures 3.8-3.10, curves are given for collision frequencies to be of 0, 1 GHz and 5 GHz, and the levels of the electron densities were lowered by 3.5. From these figures, one observes that the modeled plasma densities have to be reduced by an order of 3.2 in order to receive any signal from Antenna Location 1. Also, the plasma losses, as indicated by the collision frequency, cause only a small change on the radiation patterns, because the thicknesses of the plasma layers are quite thin in terms of a wavelength.

The input and output data files for the antenna code with the plasma are listed in Appendix B for Antenna Location 1.

3.3.2 Antenna Location 2

The geometry used to model Antenna Location 2 in the presence of the re-entry plasma is shown in Figure 3.11. The radiation patterns are shown in Figures 3.12-3.14. The onset of the patterns occurs when the levels of the electron densities are lowered by about 2.7. Since the thickness of the plasma layers are small in wavelengths, the radiation patterns show little variation with collision frequencies up to 1 GHz, as shown in Figures 3.15-3.17.

3.3.3 Antenna Location 3

For Antenna Location 3, a much more complex plasma profile than the previous two cases was simulated, as shown in Figure 3.18. Because of the planar layers with large wedge angles, only the principal plane pattern (H plane here) is meaningful. To evaluate the patterns in other planes, the

plasma profiles in these planes are required. For a more accurate solution, the actual curved surfaces of the plasma layers should be modeled in the ray-tracing approach.

The radiation patterns for Antenna Location 3 are given in Figure 3.19 for zero collision frequency. To receive any signal from Antenna Location 3, the levels of the electron densities should be reduced at least by an order of 1.4. The plasma densities are the lightest around Antenna Location 3. However, the thicknesses of the plasma layers in front of Antenna Location 3 are very thick so that the radiation signals will be attenuated considerably for a plasma profile with a high collision frequency, as shown in Figures 3.20 and 3.21, where the electron densities are lowered by $10^{1.7}$ and $10^{1.5}$, respectively.

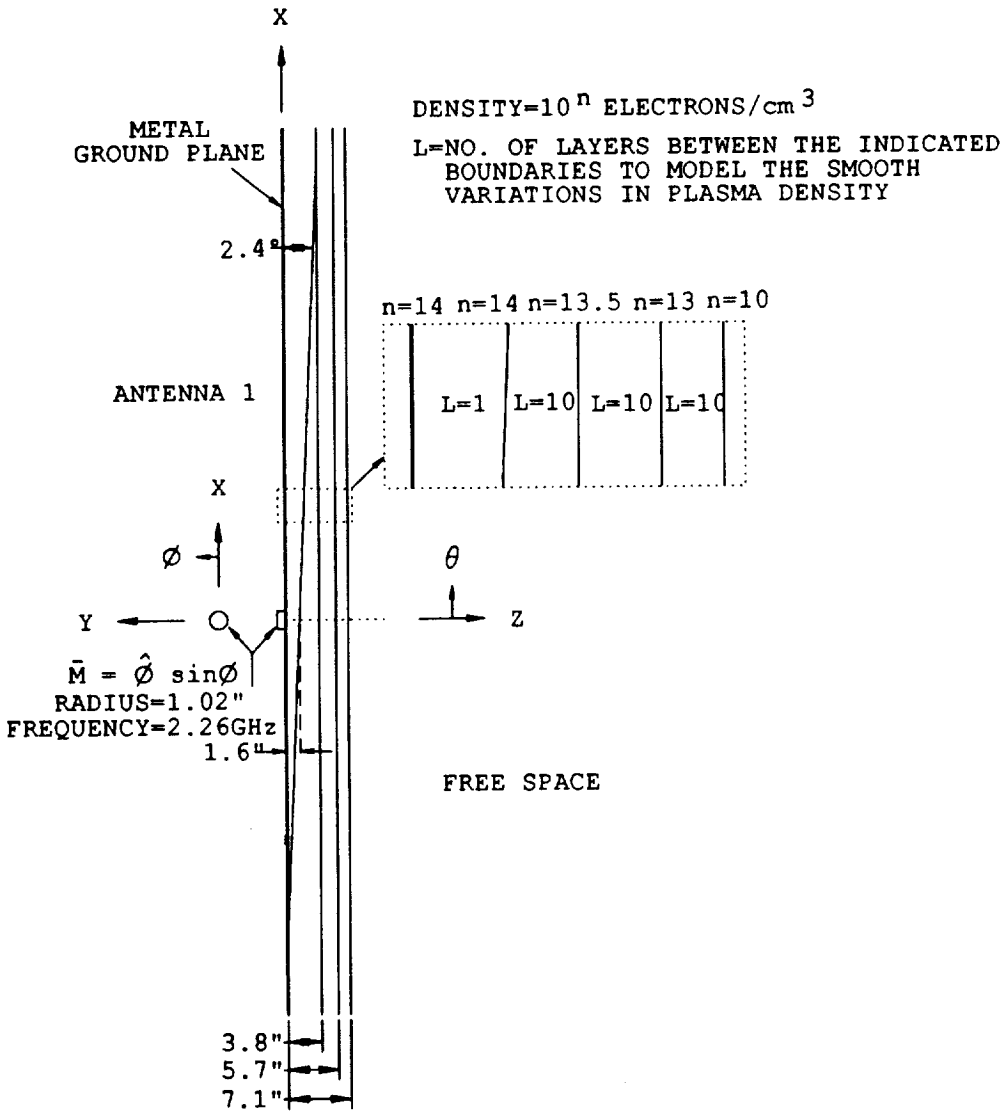

Figure 3.4: The multiple wedge-shaped layers used to simulate the AFE re-entry plasma around Antenna Location 1.

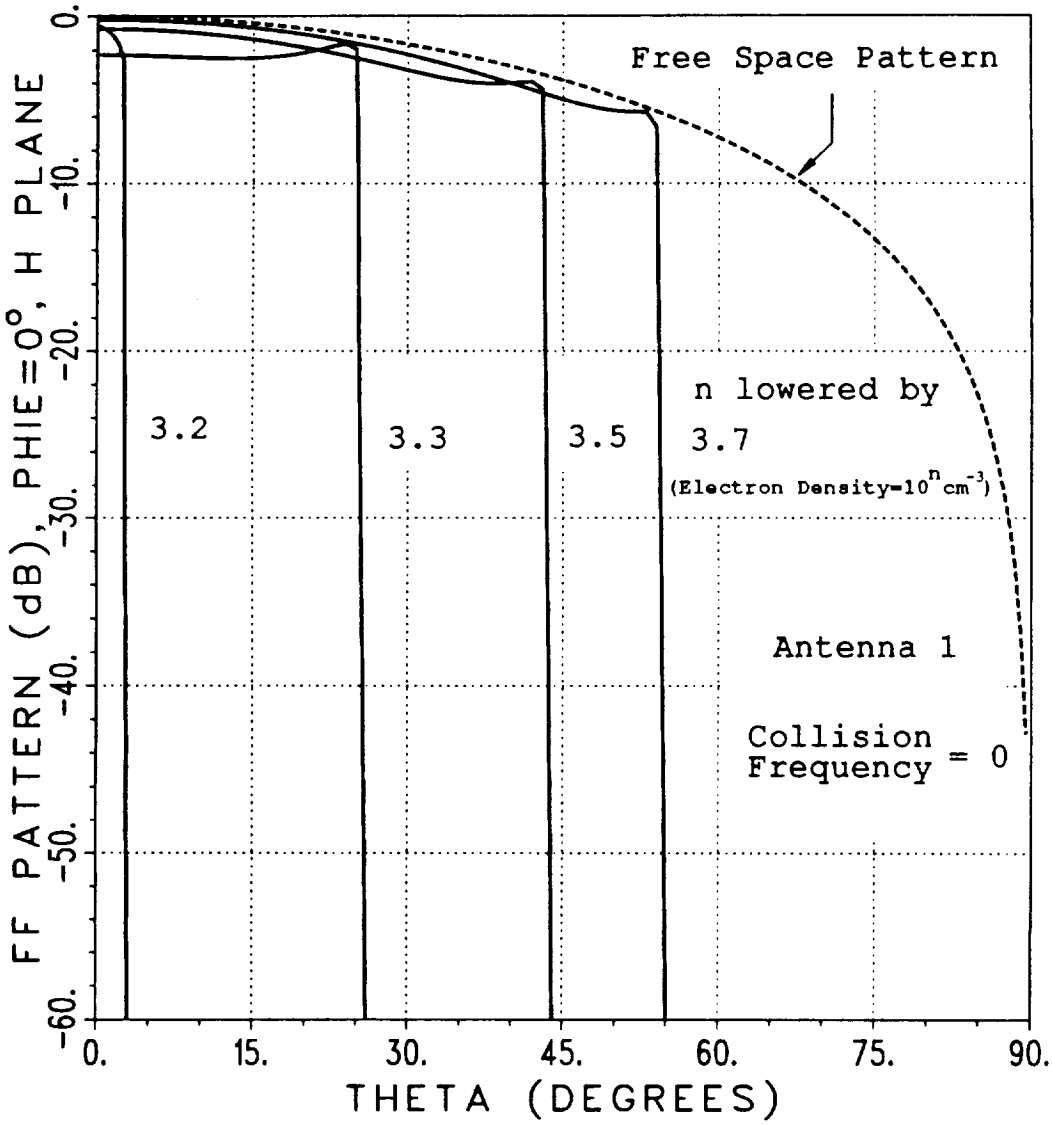

Figure 3.5: Comparison of the H-plane patterns for Antenna Location 1 radiating into plasma and free space. The electron densities of the contour lines are lowered with the values shown, and the collision frequency is zero.

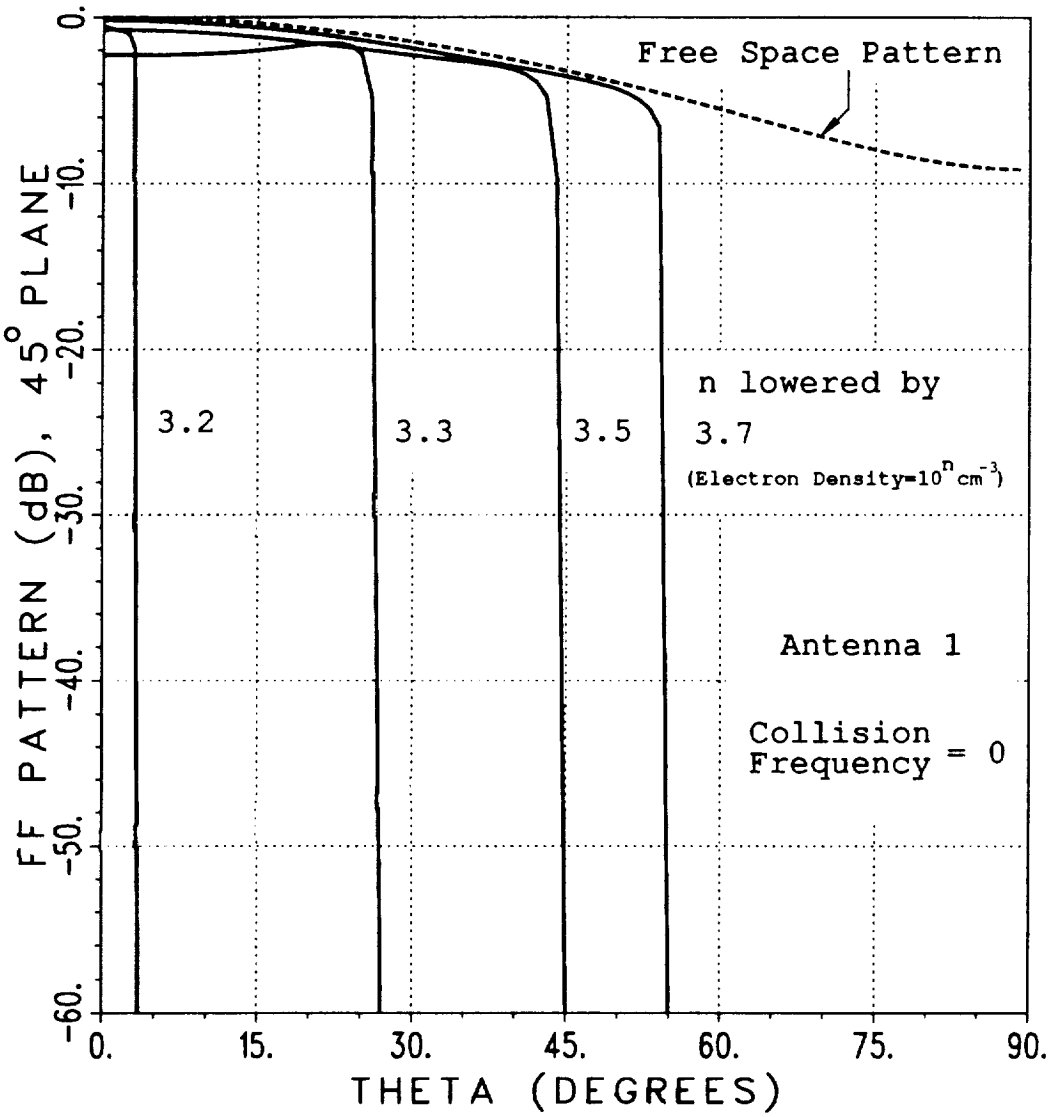

Figure 3.6: Comparison of the 45°-plane patterns for Antenna Location 1 radiating into plasma and free space. The electron densities of the contour lines are lowered with the values shown, and the collision frequency is zero.

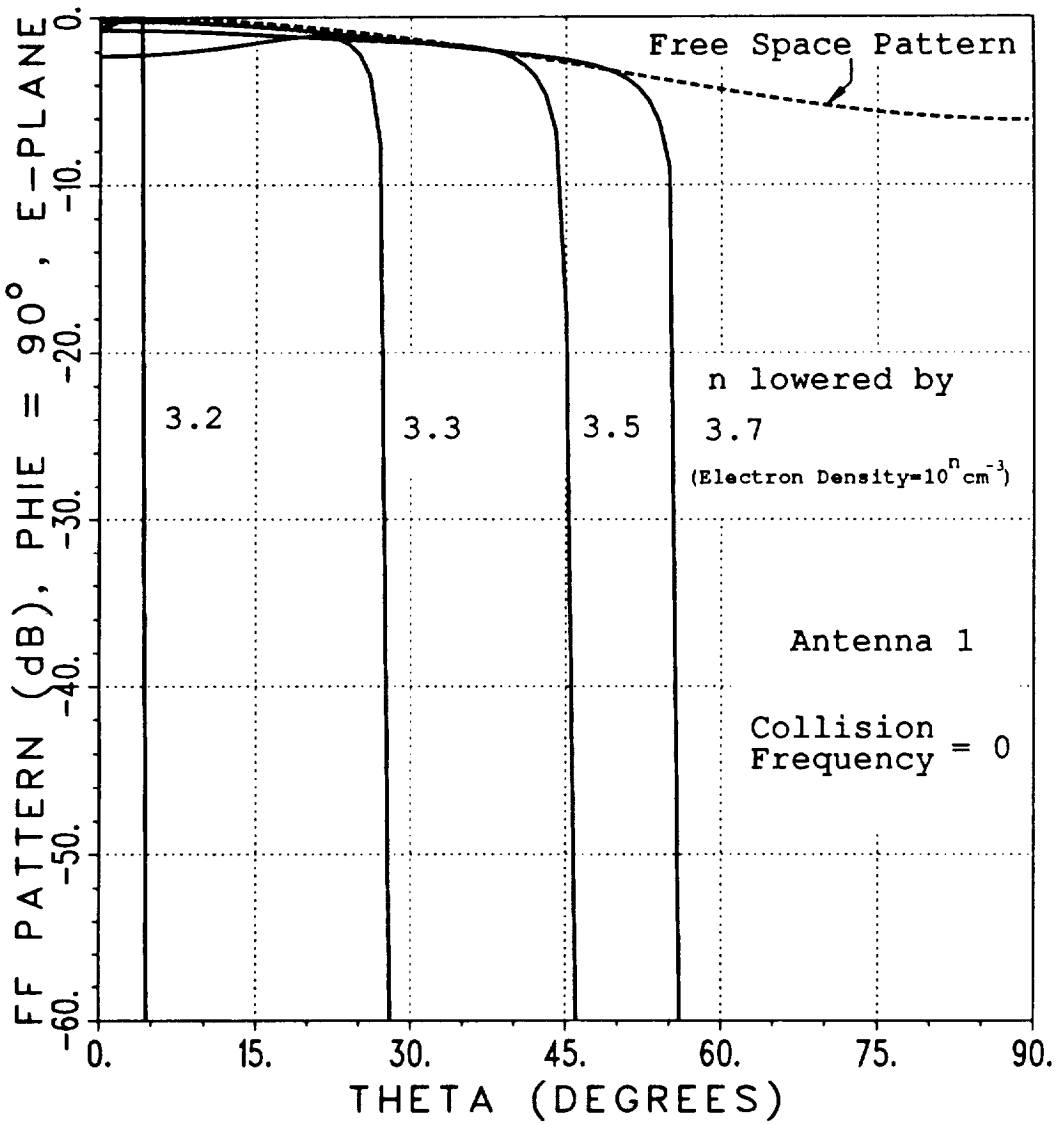

Figure 3.7: Comparison of the E-plane patterns for Antenna Location 1 radiating into plasma and free space. The electron densities of the contour lines are lowered with the values shown, and the collision frequency is zero.

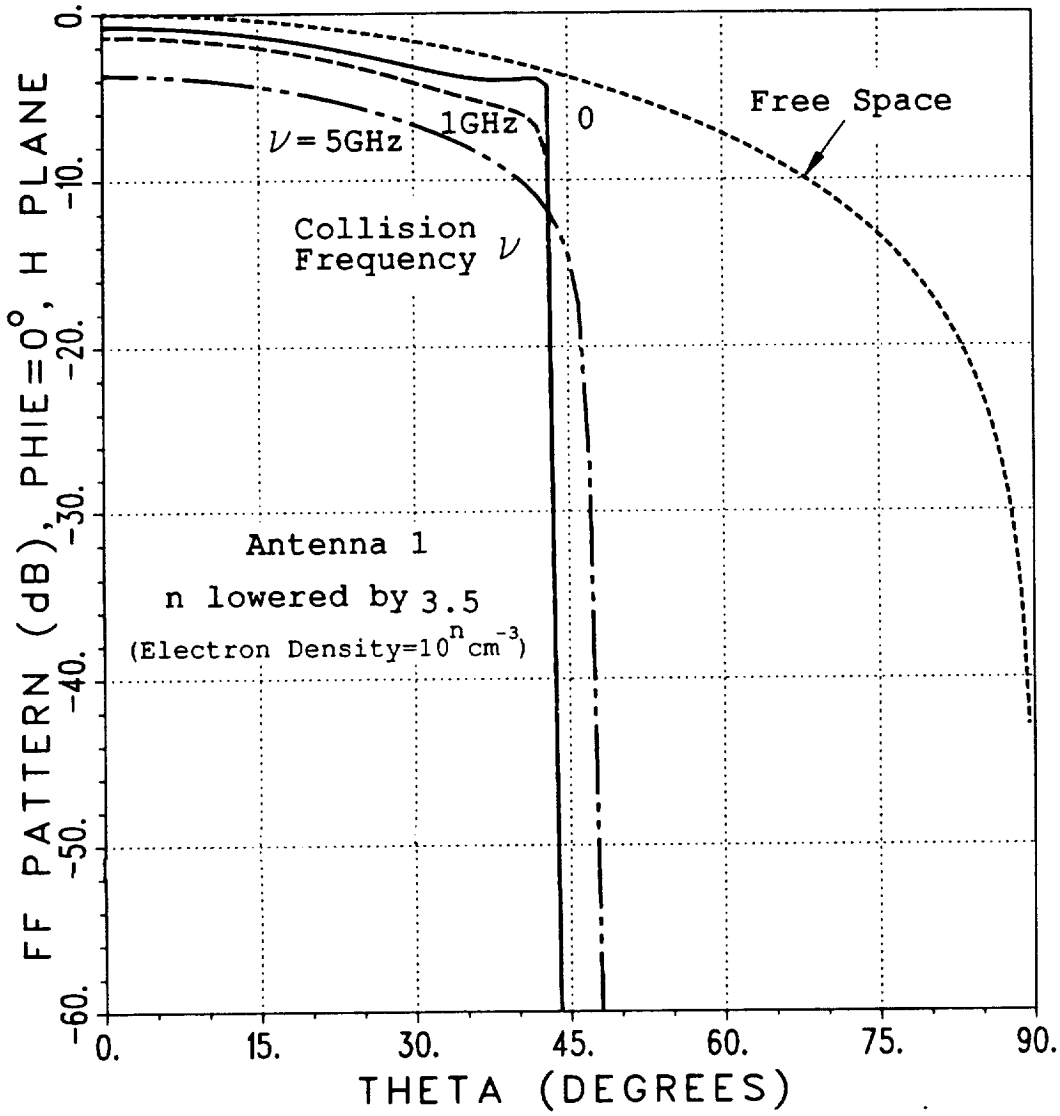

Figure 3.8: Comparison of the H-plane patterns for Antenna Location 1 radiating into plasma and free space for various collision frequencies. The electron densities of the contour lines are divided by $10^{3.5}$.

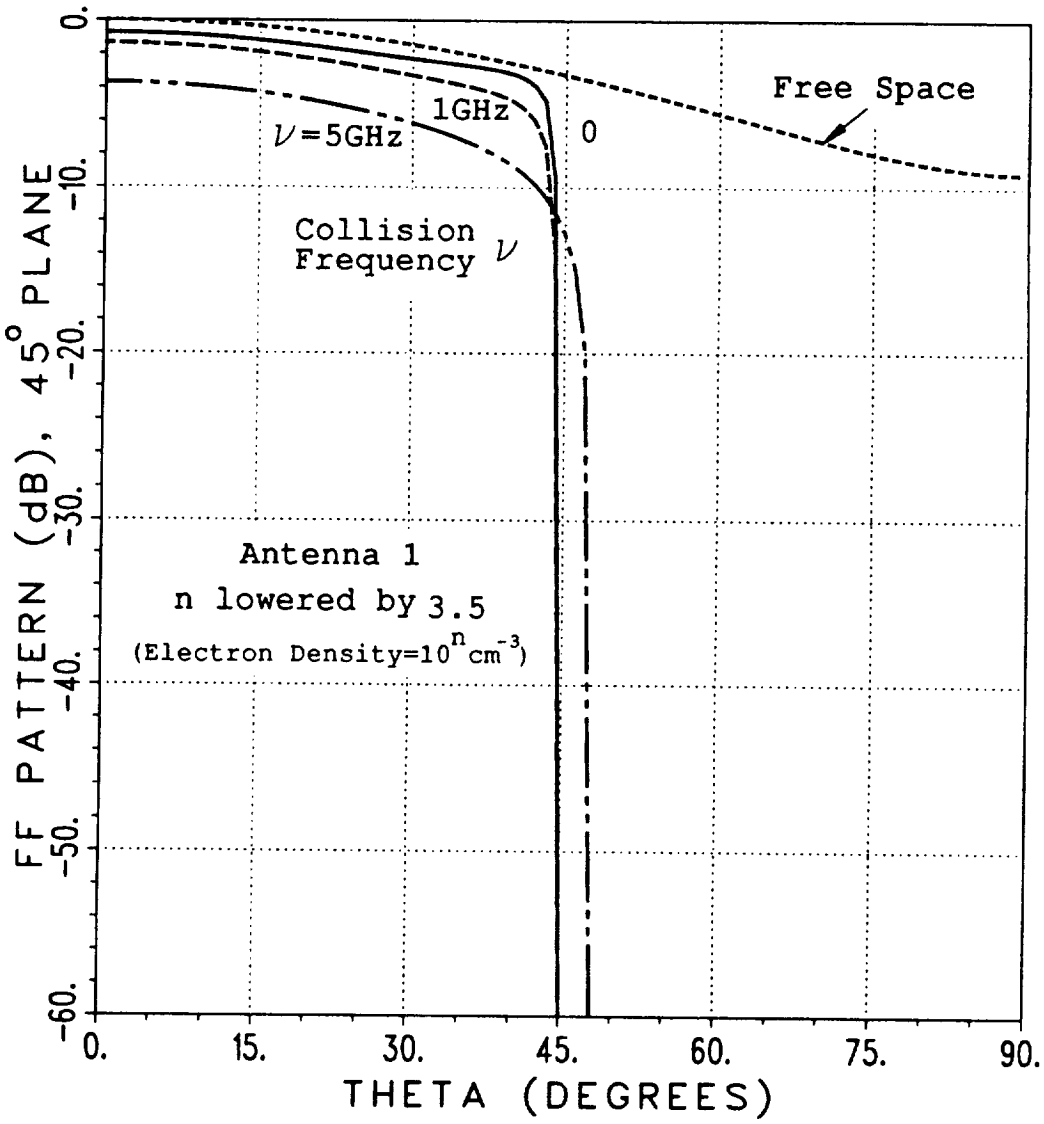

Figure 3.9: Comparison of the 45°-plane patterns for Antenna Location 1 radiating into plasma and free space for various collision frequencies. The electron densities of the contour lines are divided by $10^{3.5}$.

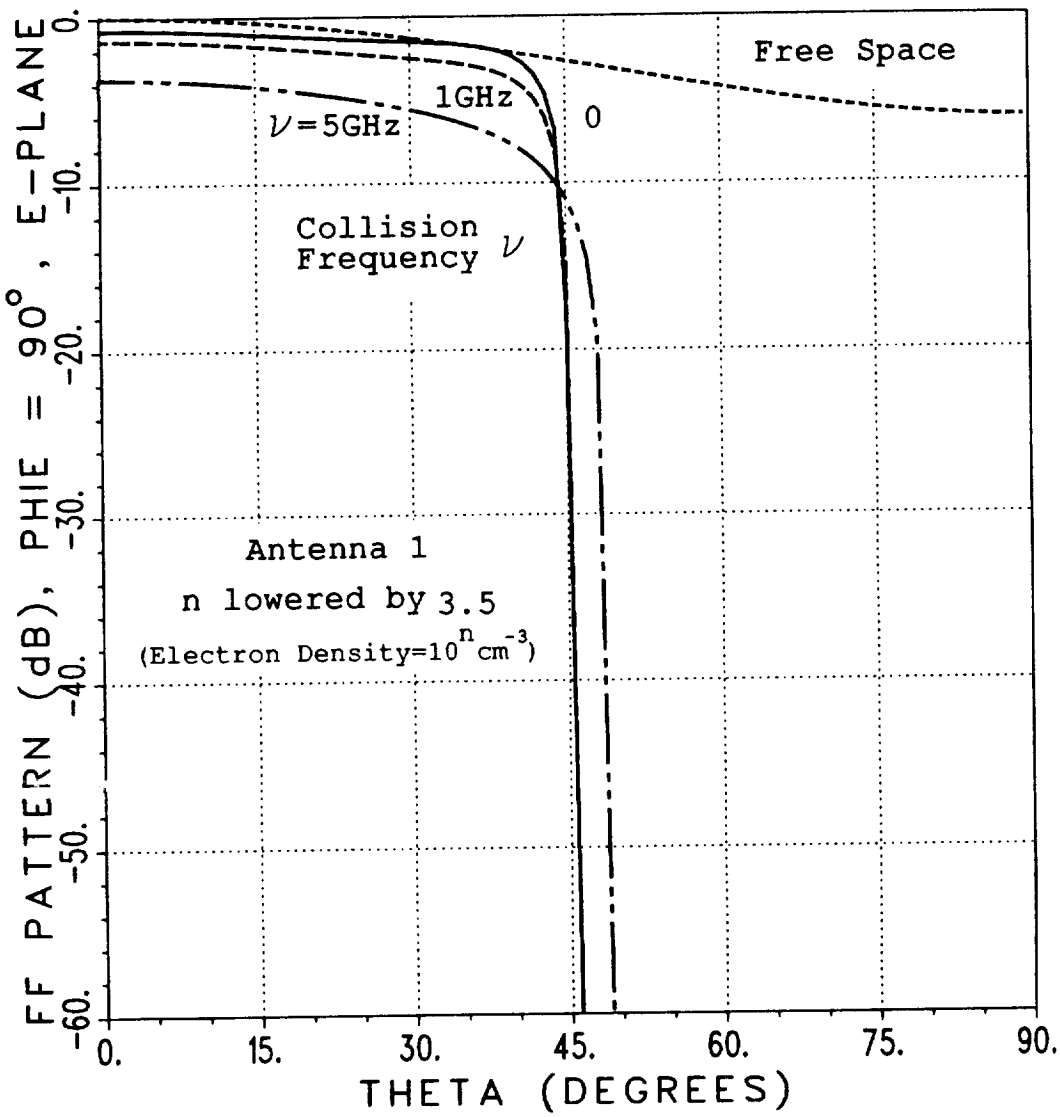

Figure 3.10: Comparison of the E-plane patterns for Antenna Location 1 radiating into plasma and free space for various collision frequencies. The electron densities of the contour lines are divided by $10^{3.5}$.

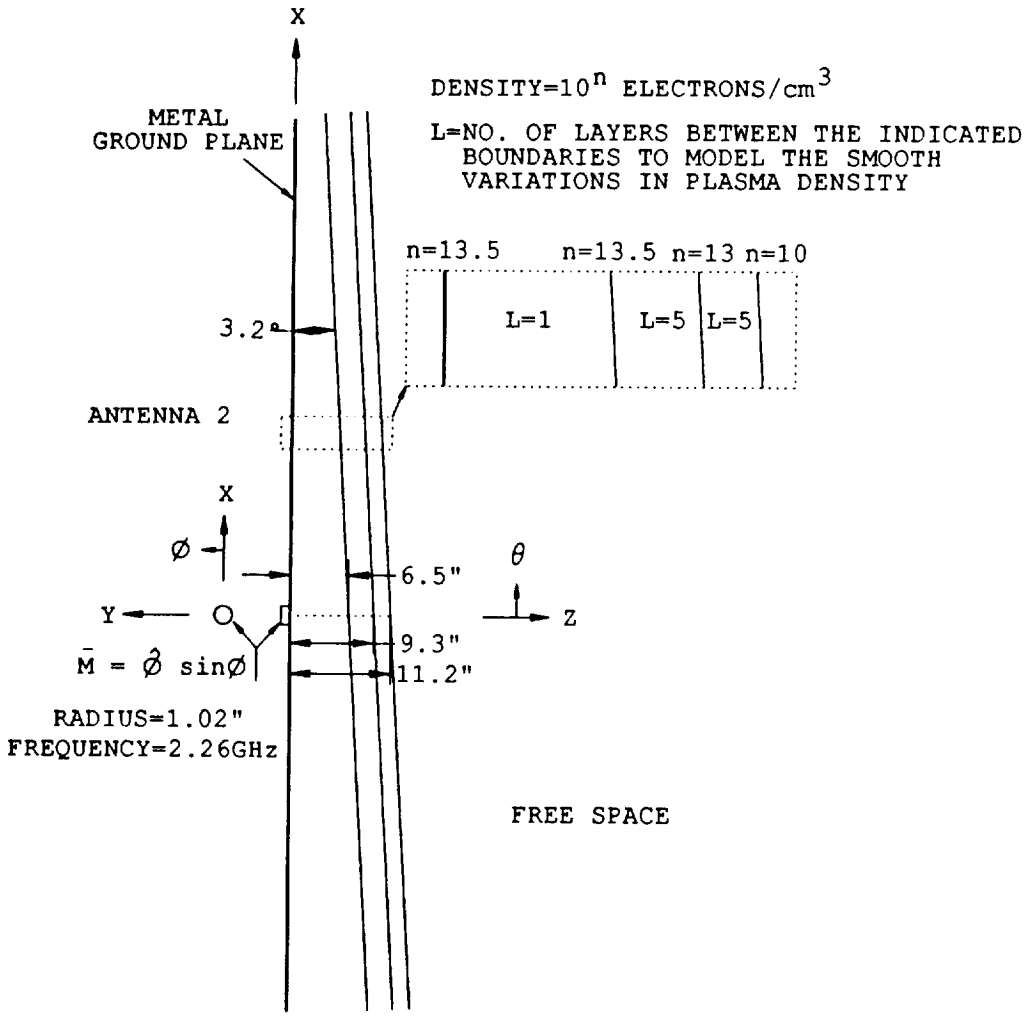

Figure 3.11: The multiple wedge-shaped layers used to simulate the AFE re-entry plasma around Antenna Location 2.

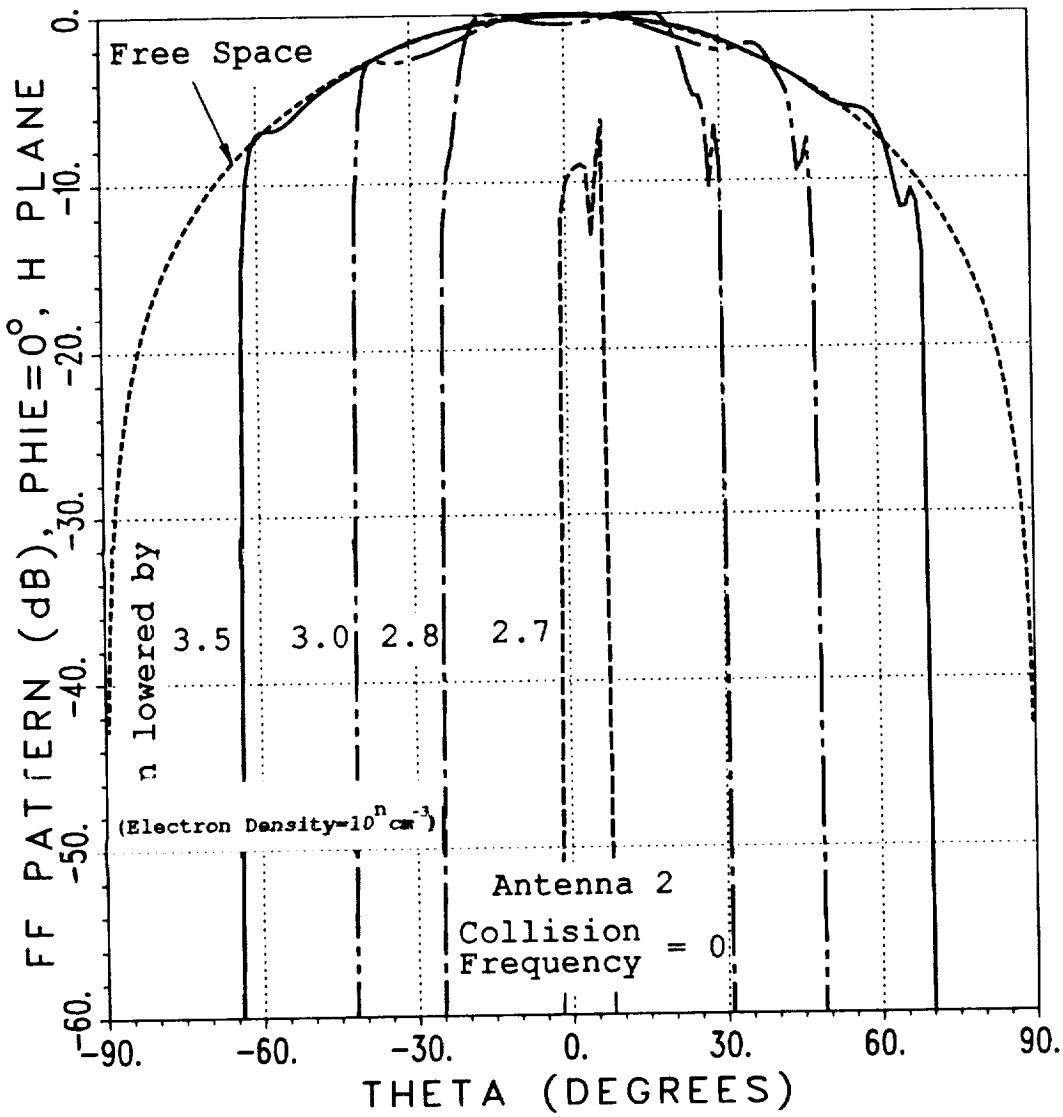

Figure 3.12: Comparison of the H-plane patterns for Antenna Location 2 radiating into plasma and free space. The electron densities of the contour lines are lowered with the values shown, and the collision frequency is zero.

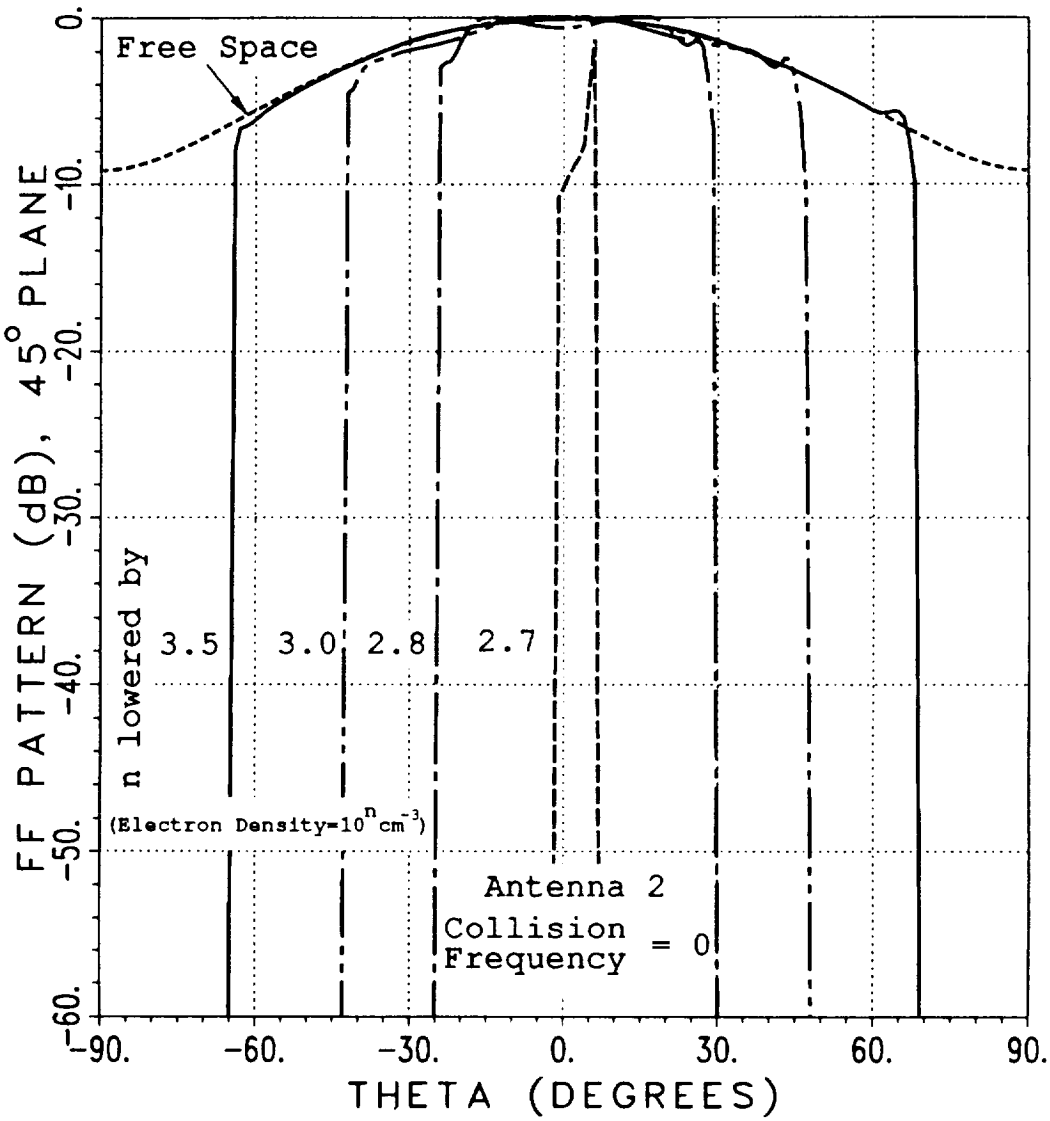

Figure 3.13: Comparison of the 45°-plane patterns for Antenna Location 2 radiating into plasma and free space. The electron densities of the contour lines are lowered with the values shown, and the collision frequency is zero.

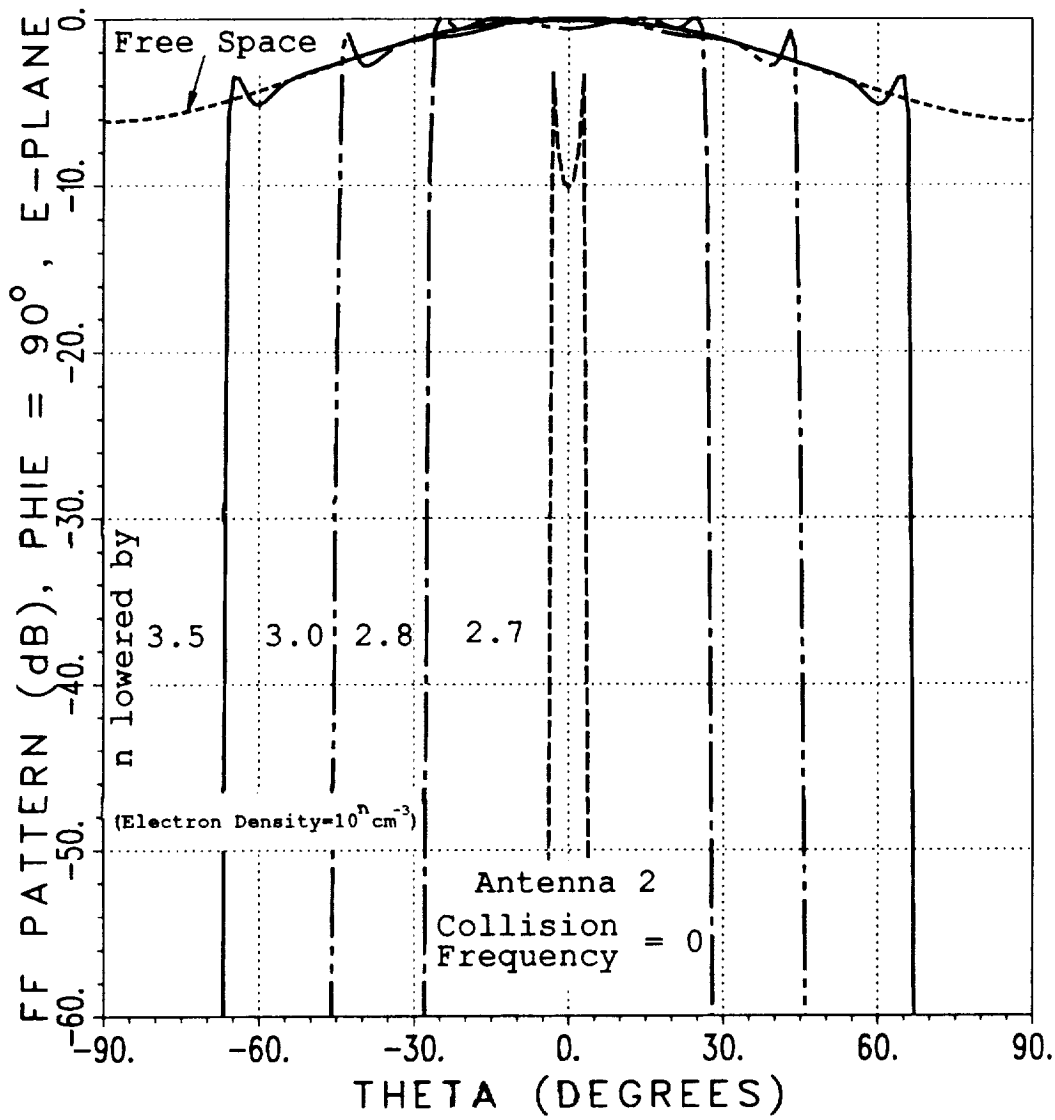

Figure 3.14: Comparison of the E-plane patterns for Antenna Location 2 radiating into plasma and free space. The electron densities of the contour lines are lowered with the values shown, and the collision frequency is zero.

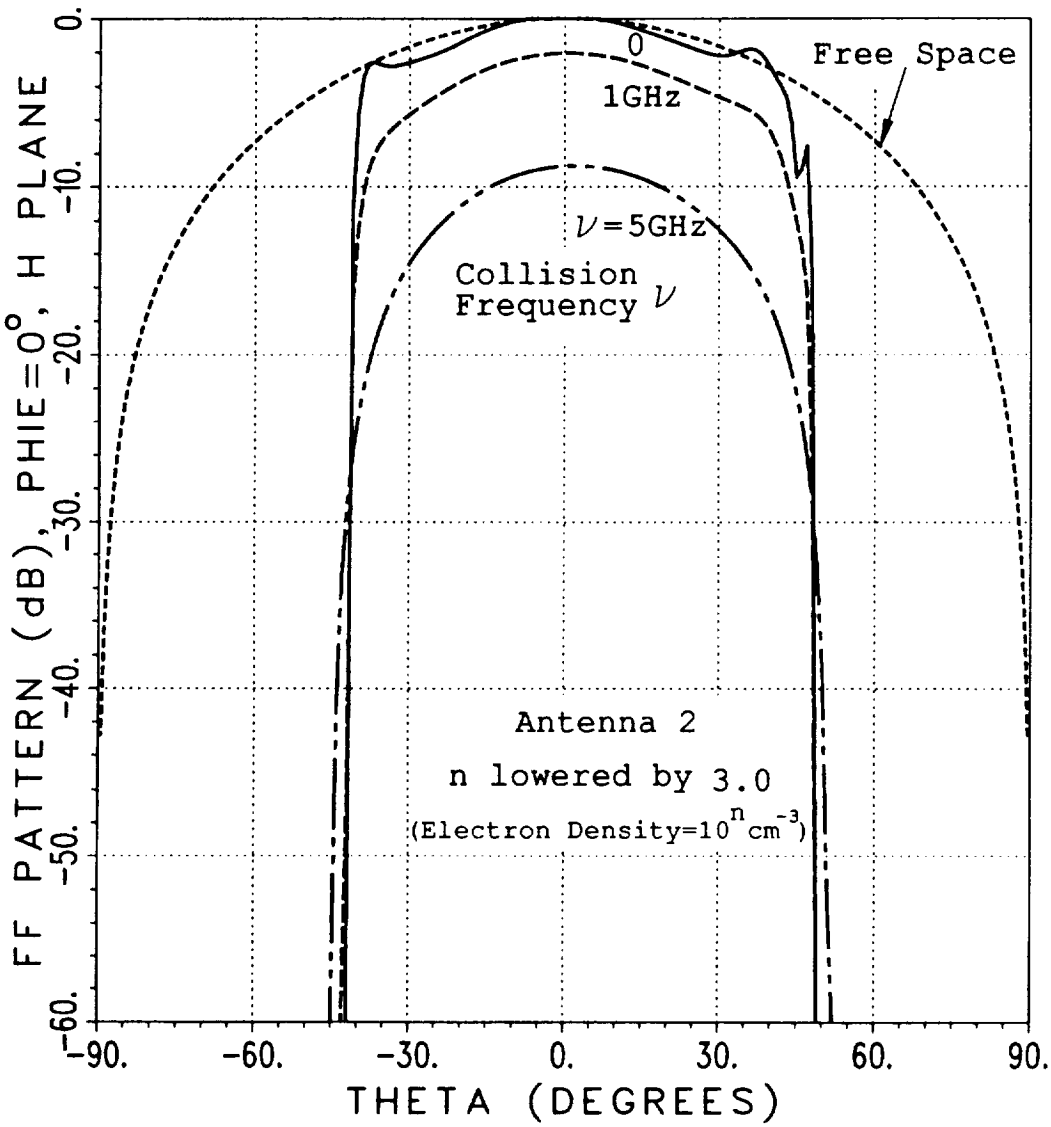

Figure 3.15: Comparison of the H-plane patterns for Antenna Location 2 radiating into plasma and free space for various collision frequencies. The electron densities of the contour lines are divided by 10^3.

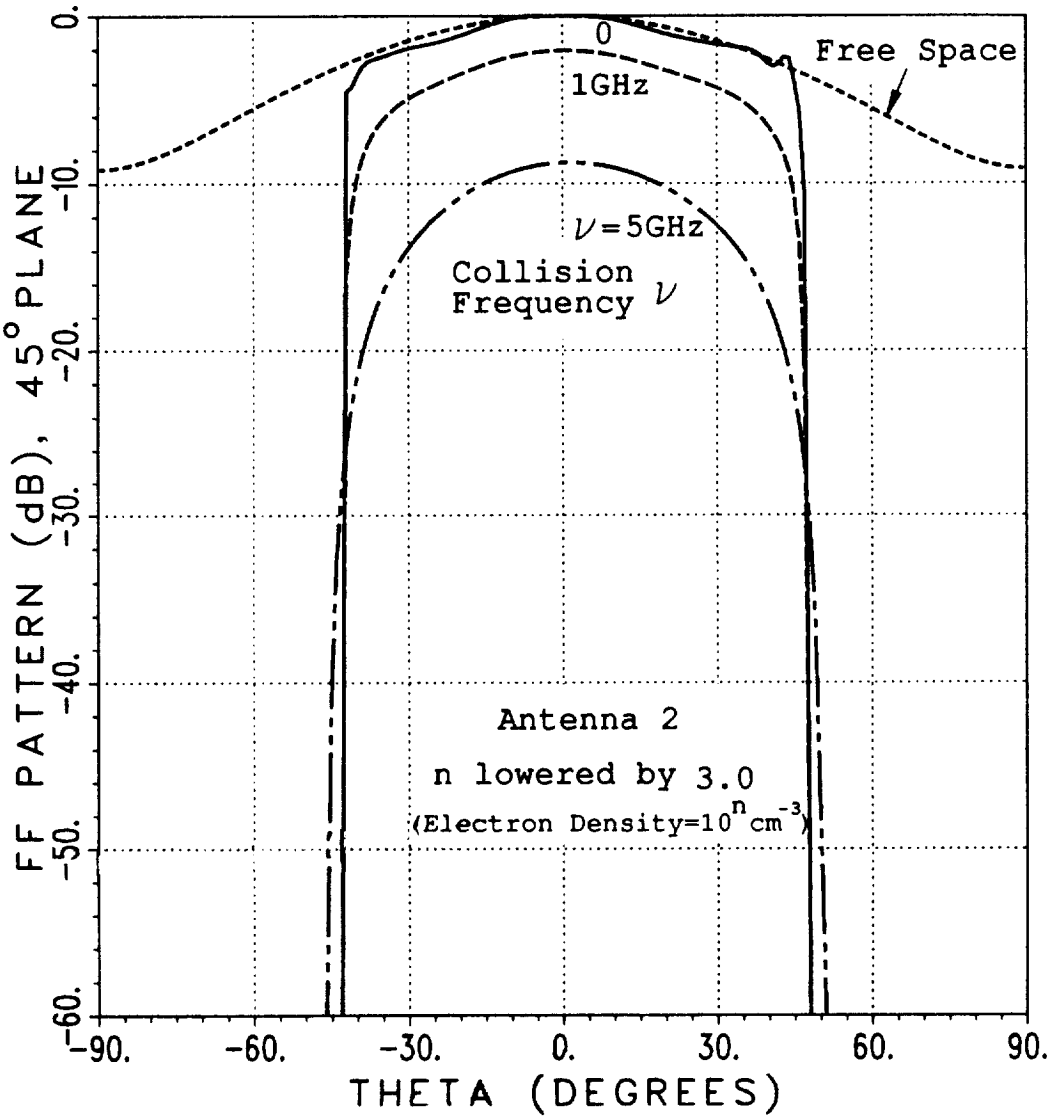

Figure 3.16: Comparison of the 45°-plane patterns for Antenna Location 2 radiating into plasma and free space for various collision frequencies. The electron densities of the contour lines are divided by 10^3.

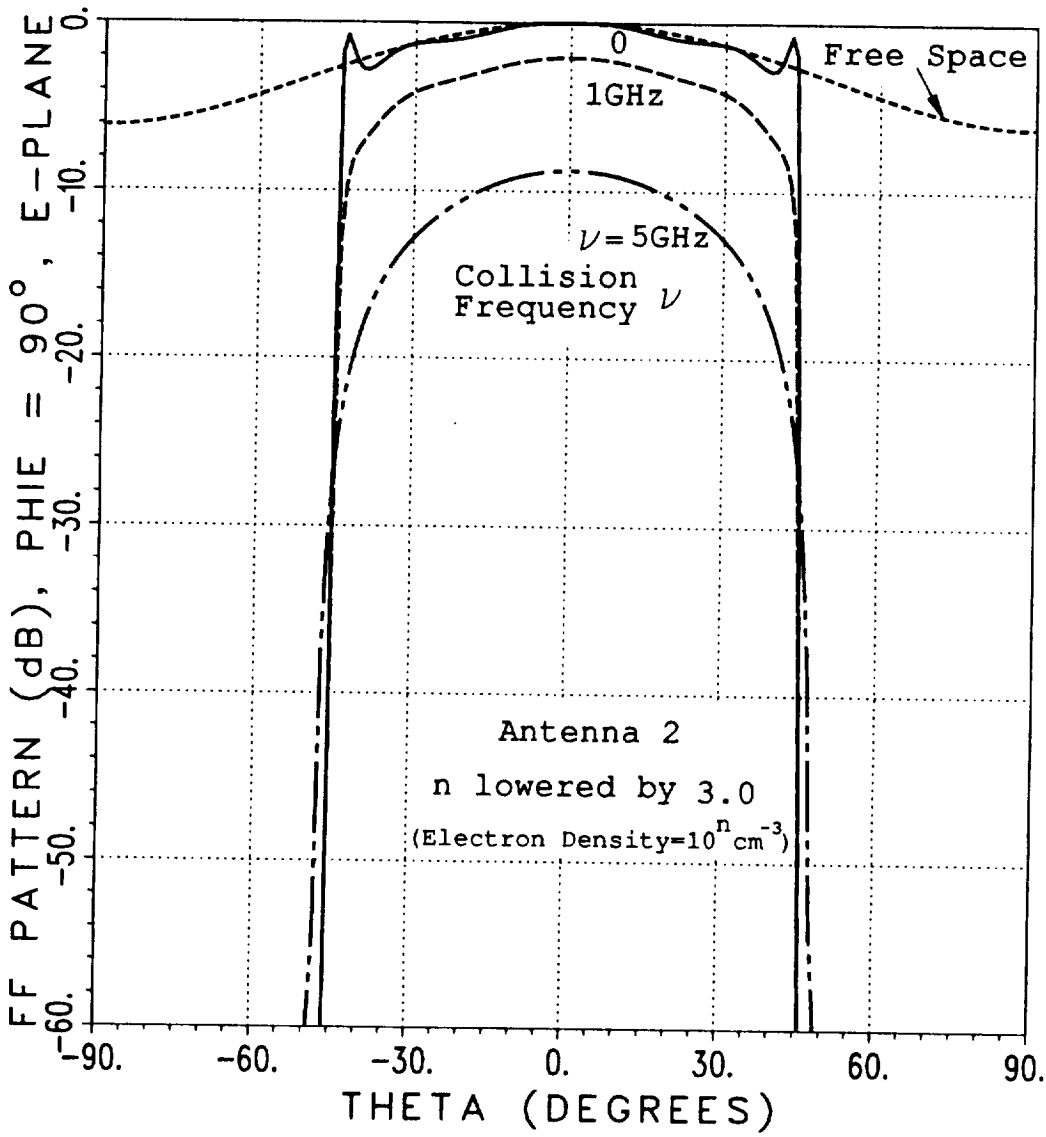

Figure 3.17: Comparison of the E-plane patterns for Antenna Location 2 radiating into plasma and free space for various collision frequencies. The electron densities of the contour lines are divided by 10^3.

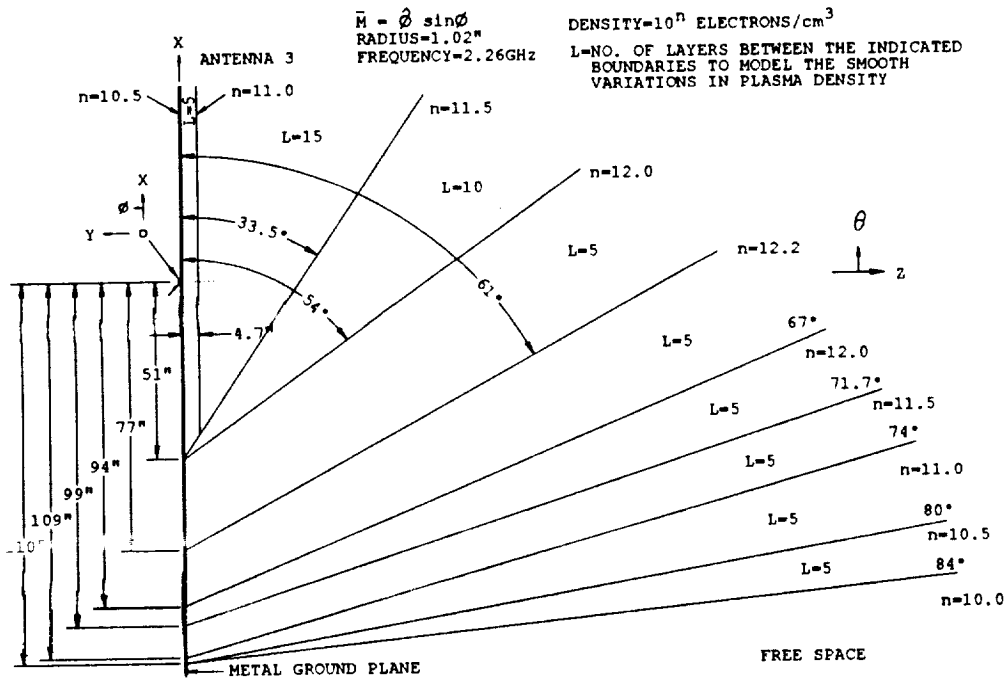

Figure 3.18: The multiple wedge-shaped layers used to simulate the AFE re-entry plasma around Antenna Location 3.

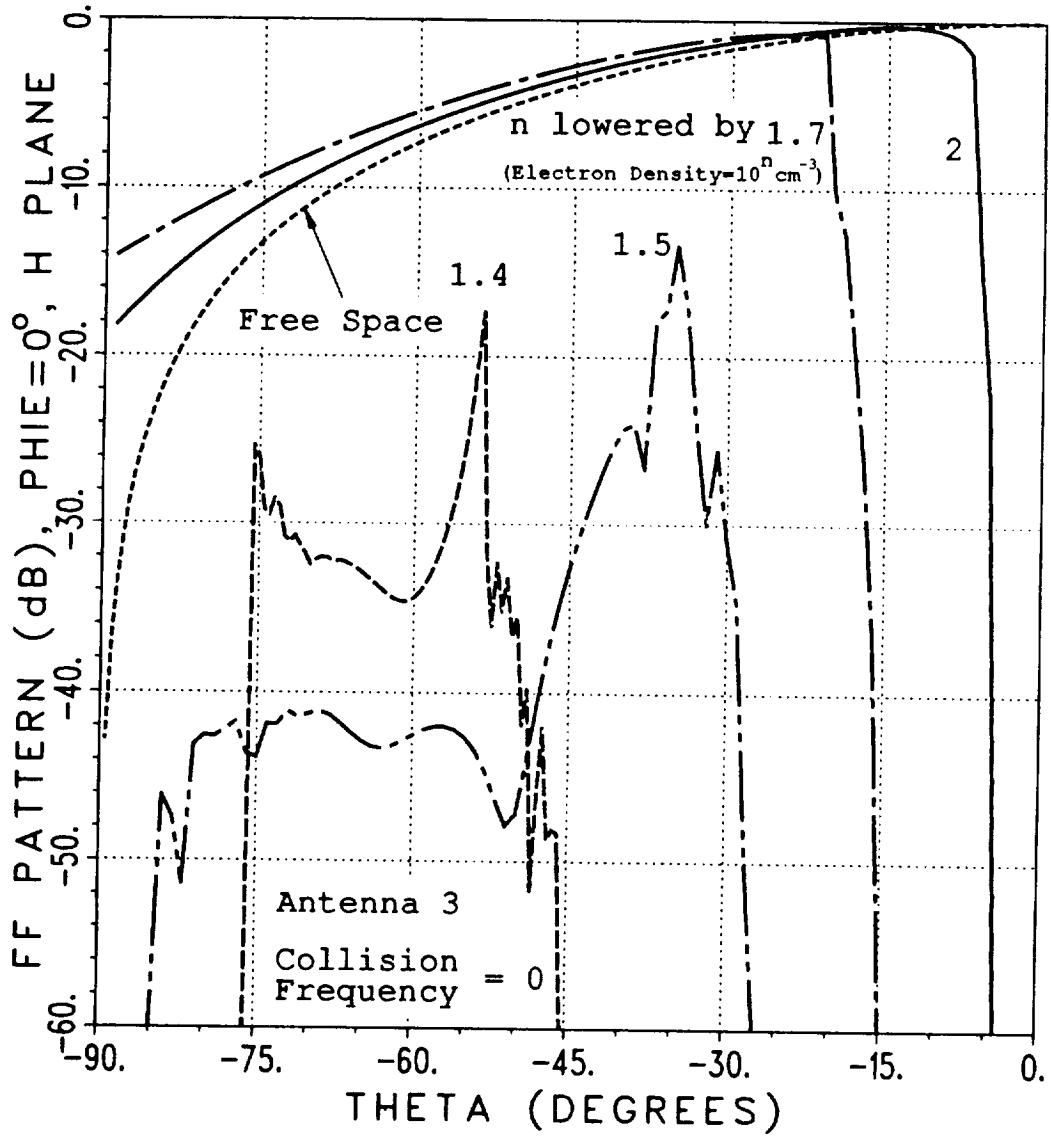

Figure 3.19: Comparison of the H-plane patterns for Antenna Location 3 radiating into plasma and free space. The electron densities of the contour lines are lowered with the values shown, and the collision frequency is zero.

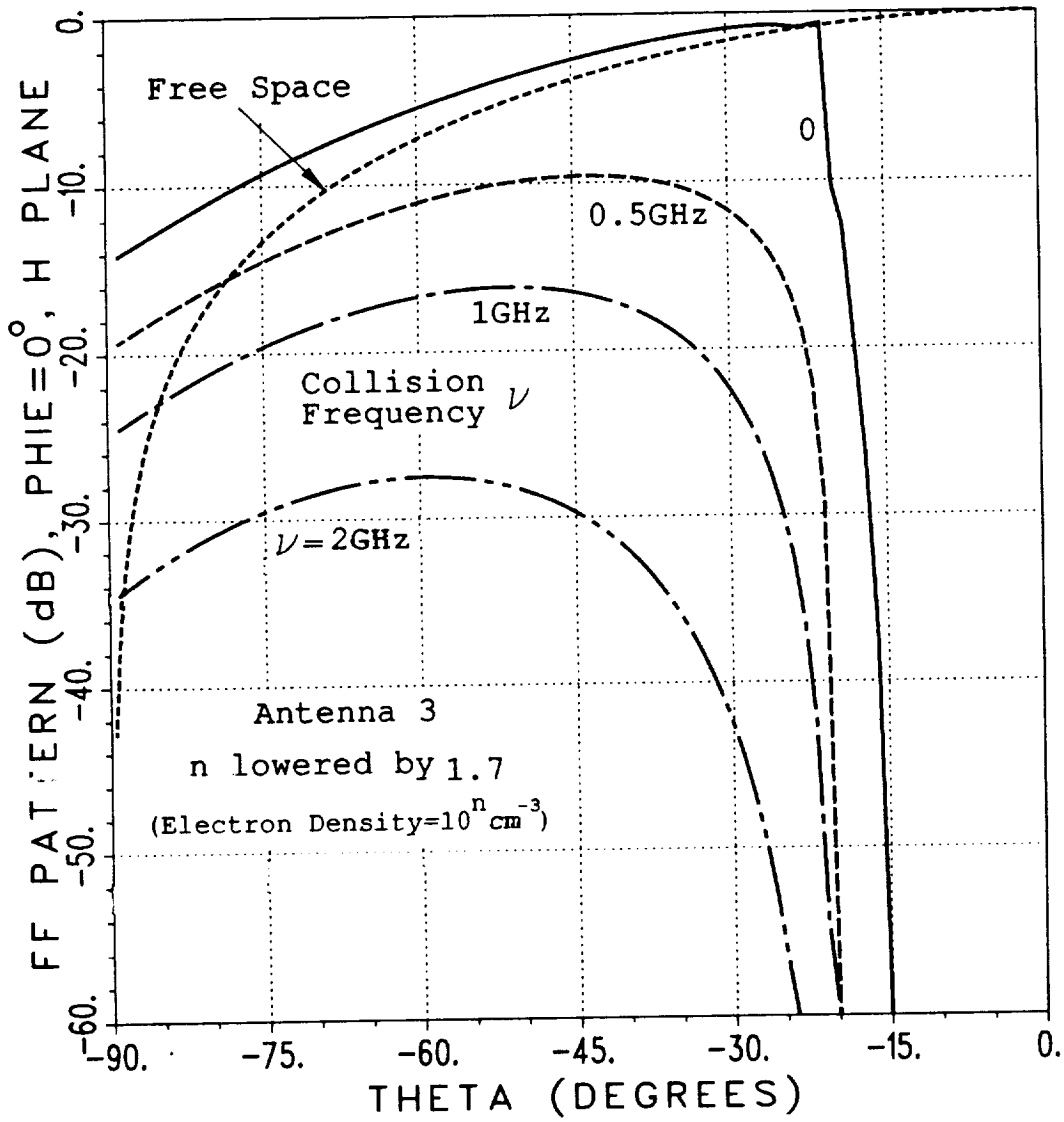

Figure 3.20: Comparison of the H-plane patterns for Antenna Location 3 radiating into plasma and free space for various collision frequencies. The electron densities of the contour lines are divided by $10^{1.7}$.

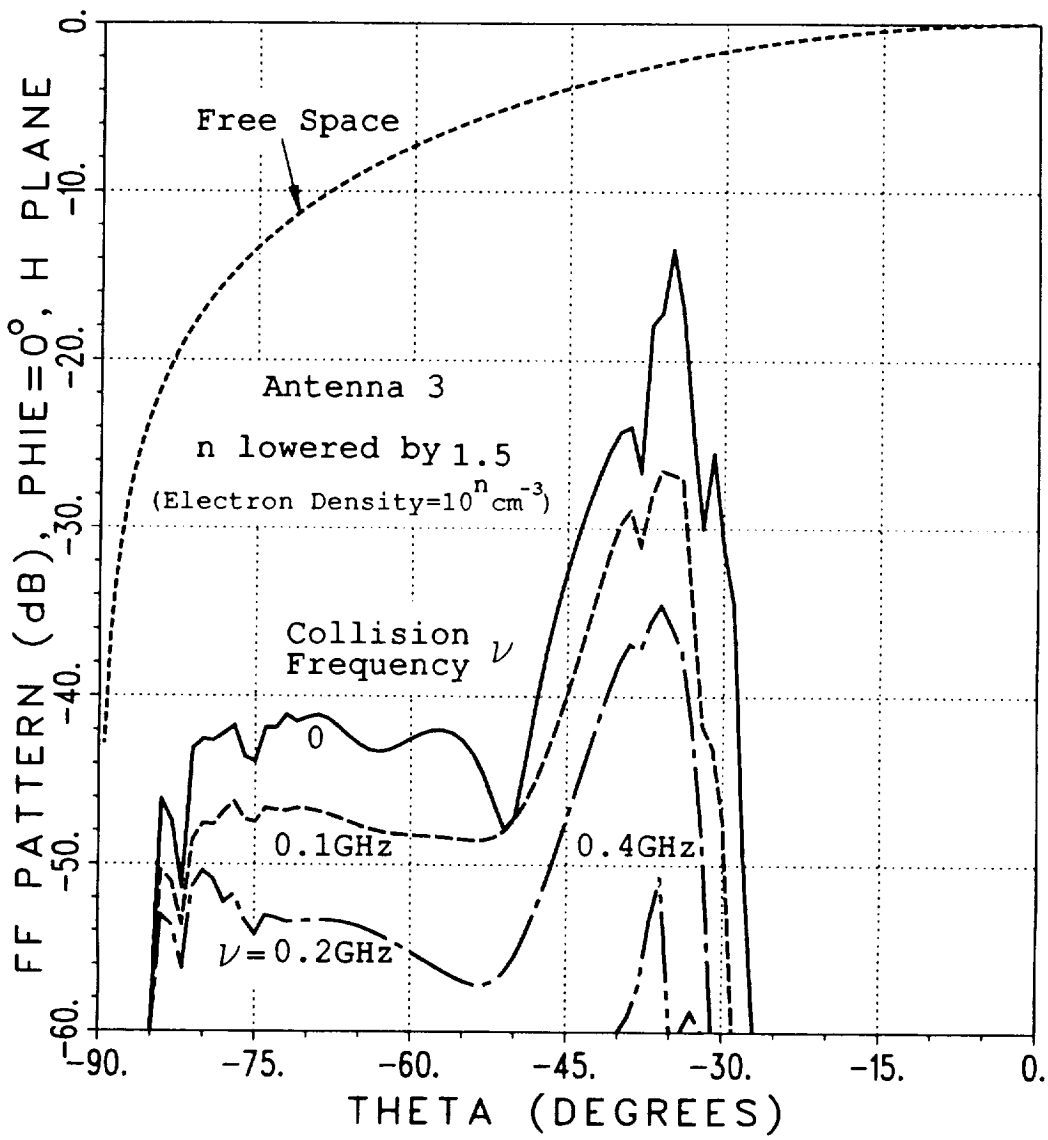

Figure 3.21: Comparison of the H-plane patterns for Antenna Location 3 radiating into plasma and free space for various collision frequencies. The electron densities of the contour lines are divided by $10^{1.5}$.

Chapter 4

Summary and Conclusions

This report describes the computer modeling for antennas on the AFE spacecraft, with and without the re-entry plasma. The free space patterns calculated from the OSU Aircraft Antenna Code were validated by data obtained from a 0.4 scale model measured at NASA Langley. The computer model provided good results for the forward half of the patterns and reasonable results for the rear half, where the signal levels are probably too low for the AFE-TDRS communications links.

Predictions are made for the antenna patterns with the effects of some expected plasma profiles. These predicted patterns were calculated by our computer code for an aperture antenna radiating into plasma layers with wedge shapes. The predictions show the pattern coverage expected under different levels of electron density and collision frequency. For Antenna Locations 1 and 2, the best transmission is expected at or near broadside ($\theta = 0$) to the spacecraft surface. For Antenna Location 3, the peak of the radiation pattern can be at a wide angle from the broadside because of the lens effect of the wedge plasma layers. Pattern coverage is expected to drop off sharply at some angle that depends on the electron density. Consequently, the pattern coverage narrows with increasing levels of the electron density. The effect of increases in the collision frequency is to further decrease the antenna pattern levels, which also results in a more

gradual drop-off in the pattern coverage. However, only the patterns from Antenna Location 3 are considerably influenced by the plasma losses. The plasma layers for the other locations are too thin to be significantly affected by the losses.

The computer code for the antenna patterns with the re-entry plasma models the spacecraft surface at the antenna location by an infinite ground plane. Although the ground plane model is not very good at wide angles in the free space patterns, it should be good for cases in which the plasma has a significant effect on the patterns. The reason for this is that the plasma will prevent pattern coverage near the spacecraft surface, as can be seen in the calculated patterns.

The present computer code has a limitation in that interactions between the aperture edge and the plasma are not modeled. This limitation should not be too serious for modeling antenna pattern coverage. However, the lack of interactions in the simulation would be a serious limitation for predicting the effect of plasma profiles on the antenna impedance. Another limitation of the computer code is the use of planar boundaries between layers. A more accurate prediction of the pattern coverage should be expected if a curved-surface model is used for those cases where the boundaries cannot be assumed as flat.

References

[1] G. D. Walberg, "A Survey of Aeroassisted Orbit Transfer," *Journal of Spacecraft and Rockets*, Vol 22, No. 1, Jan-Feb 1985, pp. 3-18.

[2] M. B. Duke, W. W. Mendel, and B. B. Roberts, "Strategies for a Permanent Lunar Base," Published in Lunar Bases and Space Activities of the 21st Century, Washington D.C., October 29-32, 1984, pp. 57-68.

[3] J. J. Jones, "The Rationale for an Aeroassisted Flight Experiment," AIAA Paper 87-1508, June 1987.

[4] J.J. Kim and W.D. Burnside, "Simulation and Analysis of Antennas Radiating in a Complex Environment," *IEEE Trans. on Antennas and Propagation*, AP-34, pp. 554-562, April 1986.

[5] C. Yang and R. C. Rudduck, "An Aperture Antenna Radiating into Wedge-Shaped Layers," Technical Report 715559-6, The Ohio State University, ElectroScience Laboratory, prepared under Contract No. NAS1-17450 for NASA, Langley Research Center, Hampton, Virginia, May 1988.

[6] Y.T. Lo, D. Solomon, and W.F. Richards, "Theory and Experiment on Microstrip Antennas," *IEEE Trans. on Antennas and Propagation*, Vol. AP-27, pp. 137-145, March 1979.

Appendix A

Input and Output Files of the OSU Aircraft Antenna Code

This is a sample input file of the Aircraft Antenna Code for E-polarization in the xz plane. All the commands are followed by a brief description of their purpose.

```
UN: UNITS IN INCHES
3
FQ: FREQUENCY = 6 GHz
1,6.,0.
FG: FUSELAGE INPUT
40.0,72.0,100.0,52.0
F
0,0,0
SG:SOURCE INFORMATION
0.,-20.0
12
0.447E+00,0.000E+00
.05,.1,0.900E+02,.1,1
0.100E+01,0.0
0.447E+00,0.300E+02
.05,.1,0.120E+03,.1,1
0.866E+00,0.0
0.447E+00,0.600E+02
.05,.1,0.150E+03,.1,1
0.500E+00,0.0
0.447E+00,0.900E+02
.05,.1,0.180E+03,.1,1
0.000E+00,0.0
```

```
0.447E+00,0.120E+03
.05,.1,0.210E+03,.1,1
-.500E+00,0.0
0.447E+00,0.150E+03
.05,.1,0.240E+03,.1,1
-.866E+00,0.0
0.447E+00,0.180E+03
.05,.1,0.270E+03,.1,1
-.100E+01,0.0
0.447E+00,0.210E+03
.05,.1,0.300E+03,.1,1
-.866E+00,0.0
0.447E+00,0.240E+03
.05,.1,0.330E+03,.1,1
-.500E+00,0.0
0.447E+00,0.270E+03
.05,.1,0.000E+00,.1,1
0.000E+00,0.0
0.447E+00,0.300E+03
.05,.1,0.300E+02,.1,1
0.500E+00,0.0
0.447E+00,0.330E+03
.05,.1,0.600E+02,.1,1
0.866E+00,0.0
PD: PATTERN
90.90.90
0,360,1
T,1000.
LP: PRINTER OUTPUT
T
EX: EXECUTE
```

This is a sample output file (Figure 2.4) from the modified aircraft code. Most of the information provided by the aircraft code was not
used, therefore a simple modification on the output routines was per-
formed to optimize calculation and processing time.

```
CM: AIR. ax=  40.0 bx =  72.0 cx = 100.0
CM:  dx =  52.0 theta pol.
CM: THC =   0.00; PHC =   0.00; THETA =  89.90
RD:
```

```
2.45
DB:
DT:
  0.000E+00   0.000E+00   0.000
  0.100E+01  -0.185E-02   0.000
  0.200E+01  -0.739E-02   0.000
  0.300E+01  -0.165E-01   0.000
  0.400E+01  -0.293E-01   0.000
  0.500E+01  -0.456E-01   0.000
  0.600E+01  -0.656E-01   0.000
  0.700E+01  -0.893E-01   0.000
  0.800E+01  -0.117E+00   0.000
  0.900E+01  -0.148E+00   0.000
.
.
.
.
  0.350E+03  -0.181E+00   0.000
  0.351E+03  -0.146E+00   0.000
  0.352E+03  -0.115E+00   0.000
  0.353E+03  -0.883E-01   0.000
  0.354E+03  -0.648E-01   0.000
  0.355E+03  -0.449E-01   0.000
  0.356E+03  -0.287E-01   0.000
  0.357E+03  -0.161E-01   0.000
  0.358E+03  -0.710E-02   0.000
  0.359E+03  -0.172E-02   0.000
  0.360E+03   0.000E+00   0.000
```

Note: Shifting the angle reference was sometimes necessary to match the reference provided by NASA.

Appendix B

Input and Output Files of the Ray Tracing Program

The command file to generate the input file for the ray tracing program to calculate the radiation patterns of Antenna 1 is the following :

```
$R THEMT_SF_WF_2_P_A1
2E-3            THRESHOLD FOR SELECTING RAYS
0. 90. 45. INI., FIN., AND INC. IN PHIE PLANES FOR TEST RAYS
-5, 80. 1. INI., FIN., AND INC. IN THETA PLANES FOR TEST RAYS
2.26E9 FREQUENCY (HZ)
0 0 : METERS    1 : INCHES
4 NO. OF REGIONS FOR DIVIDING INTO LAYERS
1 NO. OF LAYERS IN REGION 1
0.  0.04 INI. AND FIN. BOUNDARY DIST. FROM INI. BOUNDARY OF REGION
1
10 NO. OF LAYERS IN REGION 2
0.04  0.097 INI. AND FIN. BOUNDARY DIST. FROM INI. BOUNDARY OF
REGION 2
10 NO. OF LAYERS IN REGION 3
0.097  0.145 INI. AND FIN. BOUNDARY DIST. FROM INI. BOUNDARY OF
REGION 3
10 NO. OF LAYERS IN REGION 4
0.145  0.181 INI. AND FIN. BOUNDARY DIST. FROM INI. BOUNDARY OF
REGION 4
4 MAGNETIC LOOP SOURCE
0.0259 RADIUS OF THE LOOP
12 NO. OF ELEMENTS USED TO SIMULATE THE LOOP
1 A PARAMETER TO DETERMINE THE INI. POINT FOR BACKWARD TRACING
```

```
0.,90.,45. INI., FIN., AND INC. PHIE ANGLES OF THE RADIATION PATTERNS
0.,60.,1. INI., FIN., AND INC. THETA ANGLES OF THE RADIATION PATTERNS
1E-6 ANGLE OF THE RAY TUBE FOR CALCULATING SPREAD FACTOR
8 NO. OF RAYS USED FOR THE RAY TUBE
1 1 : EVEN MODE (M=SIN)  2 : ODD MODE (M=COS)
N NEED ANY CORRECTION?
```

Note:The plasma profile shown in Figure 3.4 is included in the DATA statements of THEMT_SF_WF_2_P_A1.FOR.

The following is the input file generated for the ray tracing program.

```
  2.0000001E-03
  0.0000000E+00   90.00000       45.00000
  -5.000000       80.00000       1.000000
  2.2600000E+09
           0
          32
**   Angle          Distance       Electron     Collision
**                                  Density     Frequency(Hz)
  0.0000000E+00  1.0000000E-06  0.0000000E+00  0.0000000E+00
   2.400000      4.0000997E-02  1.0000000E+20   1.000000
   2.160000      4.5700997E-02  9.4406171E+19   1.000000
   1.920000      5.1401000E-02  8.4139362E+19   1.000000
   1.680000      5.7101000E-02  7.4989420E+19   1.000000
   1.440000      6.2801003E-02  6.6834509E+19   1.000000
   1.200000      6.8501003E-02  5.9566161E+19   1.000000
  0.9600000      7.4201003E-02  5.3088490E+19   1.000000
  0.7199999      7.9901002E-02  4.7315042E+19   1.000000
  0.4800000      8.5601002E-02  4.2169649E+19   1.000000
  0.2400000      9.1301002E-02  3.7583806E+19   1.000000
 -2.3841858E-07  9.7001009E-02  3.3496514E+19   1.000000
  0.0000000E+00  0.1018010      2.9853852E+19   1.000000
  0.0000000E+00  0.1066010      2.6607203E+19   1.000000
  0.0000000E+00  0.1114010      2.3713737E+19   1.000000
  0.0000000E+00  0.1162010      2.1134927E+19   1.000000
  0.0000000E+00  0.1210010      1.8836475E+19   1.000000
  0.0000000E+00  0.1258010      1.6788055E+19   1.000000
  0.0000000E+00  0.1306010      1.4962330E+19   1.000000
  0.0000000E+00  0.1354010      1.3335215E+19   1.000000
  0.0000000E+00  0.1402010      1.1885043E+19   1.000000
  0.0000000E+00  0.1450010      1.0592528E+19   1.000000
```

```
 0.0000000E+00  0.1486010      7.0794640E+18   1.000000
 0.0000000E+00  0.1522010      3.5481276E+18   1.000000
 0.0000000E+00  0.1558010      1.7782795E+18   1.000000
 0.0000000E+00  0.1594010      8.9124859E+17   1.000000
 0.0000000E+00  0.1630010      4.4668320E+17   1.000000
 0.0000000E+00  0.1666010      2.2387132E+17   1.000000
 0.0000000E+00  0.1702010      1.1220214E+17   1.000000
 0.0000000E+00  0.1738010      5.6234131E+16   1.000000
 0.0000000E+00  0.1774010      2.8183878E+16   1.000000
 0.0000000E+00  0.1810010      1.4125363E+16   1.000000
 2.5900001E-02          -1          12
 2.4835269E-09  0.3160184
  1.000000
 0.0000000E+00   60.00000       1.000000
 0.0000000E+00   90.00000       45.00000
 1.0000000E-06           8
(0.0000000E+00,0.0000000E+00) (-1.3351440E-05,0.0000000E+00)
 2.5900001E-02  0.0000000E+00
(0.2736915,0.0000000E+00) (0.1580025,0.0000000E+00)
 2.2430059E-02  1.2950000E-02
(0.2736914,0.0000000E+00) (0.4740342,0.0000000E+00)
 1.2949999E-02  2.2430060E-02
(-2.7628365E-08,0.0000000E+00) (0.6320500,0.0000000E+00)
-1.1321249E-09  2.5900001E-02
(-0.2736915,0.0000000E+00) (0.4740341,0.0000000E+00)
-1.2950002E-02  2.2430059E-02
(-0.2736914,0.0000000E+00) (0.1580024,0.0000000E+00)
-2.2430060E-02  1.2949997E-02
(2.0595238E-07,0.0000000E+00) (-1.3351440E-05,0.0000000E+00)
-2.5900001E-02 -8.4392919E-09
(0.2736916,0.0000000E+00) (0.1580027,0.0000000E+00)
-2.2430051E-02 -1.2950012E-02
(0.2736913,0.0000000E+00) (0.4740345,0.0000000E+00)
-1.2949987E-02 -2.2430066E-02
(-3.0892858E-07,0.0000000E+00) (0.6320500,0.0000000E+00)
 1.2658938E-08 -2.5900001E-02
(-0.2736916,0.0000000E+00) (0.4740340,0.0000000E+00)
 1.2950010E-02 -2.2430053E-02
(-0.2736914,0.0000000E+00) (0.1580023,0.0000000E+00)
 2.2430062E-02 -1.2949994E-02
    LOOP    ;32 LAYERS ; FREQ =  2.26 GHz ; R= 0.02590
```

Note:The collision frequency can be changed by editing the above file.

The orders of the electron densities to be reduced are read from terminal.

The output file of the ray tracing program, THEMT_SF_2_P_A1.FOR, with electron densities reduced by 1E3.5 and 1GHz collision frequency (Figure 3.8) is given below :

ANT#1, M=sin(phie), R=1.0195", Ground Plane, Freq=2.26GHZ, Collision Freq=1GHz, Ne/1E3.5

3	61
0.0000000E+00	
0.0000000E+00	3.236477
1.000000	3.234979
2.000000	3.231341
3.000000	3.225659
4.000000	3.217806
5.000000	3.207858
6.000000	3.195836
7.000000	3.181690
8.000000	3.165408
9.000000	3.147143
10.00000	3.126692
11.00000	3.104270
12.00000	3.079733
13.00000	3.053173
14.00000	3.024617
15.00000	2.994079
16.00000	2.961618
17.00000	2.927207
18.00000	2.890975
19.00000	2.852899
20.00000	2.813105
21.00000	2.771635
22.00000	2.728676
23.00000	2.684229
24.00000	2.638447
25.00000	2.591505
26.00000	2.543572
27.00000	2.494843
28.00000	2.445669
29.00000	2.396187
30.00000	2.346786
31.00000	2.297795

32.00000	2.249687
33.00000	2.202790
34.00000	2.157633
35.00000	2.114475
36.00000	2.073511
37.00001	2.034757
38.00001	1.997196
39.00001	1.958612
40.00001	1.913358
41.00001	1.847616
42.00001	1.723143
43.00001	1.389351
44.00002	0.0000000E+00
45.00002	0.0000000E+00
46.00002	0.0000000E+00
47.00002	0.0000000E+00
48.00002	0.0000000E+00
49.00002	0.0000000E+00
50.00002	0.0000000E+00
51.00002	0.0000000E+00
52.00002	0.0000000E+00
53.00002	0.0000000E+00
54.00003	0.0000000E+00
55.00003	0.0000000E+00
56.00003	0.0000000E+00
57.00003	0.0000000E+00
58.00003	0.0000000E+00
59.00003	0.0000000E+00
60.00003	0.0000000E+00
45.00000	
0.0000000E+00	3.236477
1.000000	3.235322
2.000000	3.232419
3.000000	3.227867
4.000000	3.221533
5.000000	3.213564
6.000000	3.203891
7.000000	3.192596
8.000000	3.179656
9.000000	3.165121
10.00000	3.148975
11.00000	3.131365
12.00000	3.112259
13.00000	3.091682
14.00000	3.069839

15.00000	3.046576
16.00000	3.022077
17.00000	2.996448
18.00000	2.969708
19.00000	2.942019
20.00000	2.913365
21.00000	2.883882
22.00000	2.853669
23.00000	2.822896
24.00000	2.791610
25.00000	2.759950
26.00000	2.727876
27.00000	2.695760
28.00000	2.663374
29.00000	2.631069
30.00000	2.598587
31.00000	2.566068
32.00000	2.533259
33.00000	2.499995
34.00000	2.465887
35.00000	2.430248
36.00000	2.392108
37.00001	2.349900
38.00001	2.301172
39.00001	2.241945
40.00001	2.165425
41.00001	2.058729
42.00001	1.894253
43.00001	1.595320
44.00002	0.7762950
45.00002	0.0000000E+00
46.00002	0.0000000E+00
47.00002	0.0000000E+00
48.00002	0.0000000E+00
49.00002	0.0000000E+00
50.00002	0.0000000E+00
51.00002	0.0000000E+00
52.00002	0.0000000E+00
53.00002	0.0000000E+00
54.00003	0.0000000E+00
55.00003	0.0000000E+00
56.00003	0.0000000E+00
57.00003	0.0000000E+00
58.00003	0.0000000E+00
59.00003	0.0000000E+00

60.00003	0.0000000E+00
90.00000	
0.0000000E+00	3.236477
1.000000	3.235800
2.000000	3.233885
3.000000	3.230608
4.000000	3.226098
5.000000	3.220185
6.000000	3.213106
7.000000	3.204920
8.000000	3.195510
9.000000	3.184962
10.00000	3.173419
11.00000	3.160815
12.00000	3.147390
13.00000	3.133044
14.00000	3.118025
15.00000	3.102239
16.00000	3.085905
17.00000	3.069069
18.00000	3.051884
19.00000	3.034344
20.00000	3.016709
21.00000	2.998756
22.00000	2.980881
23.00000	2.963022
24.00000	2.945347
25.00000	2.927707
26.00000	2.910117
27.00000	2.892737
28.00000	2.875315
29.00000	2.857711
30.00000	2.839570
31.00000	2.820822
32.00000	2.800712
33.00000	2.778680
34.00000	2.753813
35.00000	2.724821
36.00000	2.690135
37.00001	2.647511
38.00001	2.593766
39.00001	2.524572
40.00001	2.433352
41.00001	2.310234
42.00001	2.138266

43.00001	1.887030
44.00002	1.489498
45.00002	0.6983163
46.00002	0.0000000E+00
47.00002	0.0000000E+00
48.00002	0.0000000E+00
49.00002	0.0000000E+00
50.00002	0.0000000E+00
51.00002	0.0000000E+00
52.00002	0.0000000E+00
53.00002	0.0000000E+00
54.00003	0.0000000E+00
55.00003	0.0000000E+00
56.00003	0.0000000E+00
57.00003	0.0000000E+00
58.00003	0.0000000E+00
59.00003	0.0000000E+00
60.00003	0.0000000E+00

PAGE _____ INTENTIONALLY BLANK

NASA
National Aeronautics and Space Administration

Report Documentation Page

1. Report No.	2. Government Accession No.	3. Recipient's Catalog No.
NASA CR-4409		

4. Title and Subtitle	5. Report Date
Prediction of the Pattern Performance for the Aeroassist Flight Experiment (AFE) Spacecraft	October 1991
	6. Performing Organization Code

7. Author(s)	8. Performing Organization Report No.
C. Yang R. Rudduck R. Torres	715559-7
	10. Work Unit No.
	592-01-11-12
9. Performing Organization Name and Address	11. Contract or Grant No.
Ohio State University ElectroScience Laboratory 1320 Kinnear Road Columbus, Ohio 43212	NAS1-17450
	13. Type of Report and Period Covered
12. Sponsoring Agency Name and Address	Contractor Report (Final Report)
National Aeronautics and Space Administration Langley Research Center Hampton, Virginia 23665-5225	14. Sponsoring Agency Code

15. Supplementary Notes

Langley Technical Task Monitor: Thomas G. Campbell

16. Abstract

Recent studies by the National Aeronautics and Space Administration (NASA) have focused attention on a class of missions in which a reusable Aeroassisted Orbit Transfer Vehicle (AOTV) would be used for the delivery and return of cargo, servicing equipment, and personnel between low and high Earth orbit or the moon. On return from high orbit, these vehicles traveling at a speed of approximately 34,000 ft/sec will fly a roll-modulated trajectory with a perigee of 250,000 to 300,000-ft altitude, skip back out of the atmosphere, and rendezvous with a Space Station in low Earth orbit. In order to provide a set of benchmark flight data for AOTV applications, NASA has undertaken the development of an Aeroassisted Flight Experiment (AFE) which will be launched from the Space Shuttle. A representative aeroassist trajectory will be flown and sensor measurements of aerodynamic performance, thermal protection response, and plasma ionization reentry effects will be obtained. The research reported here concerns the spacecraft antenna and provides estimates of signal transmissions from the AFE to the Tracking and Data Relay Satellites (TDRS) during the reentry period. The computer modeling of the antennas on the spacecraft is presented with and without the reentry plasma.

17. Key Words (Suggested by Author(s))	18. Distribution Statement
antennas Aeroassist Flight Experiment aerobraking plasma physics	unclassified - unlimited subject category 17

19. Security Classif. (of this report)	20. Security Classif. (of this page)	21. No. of pages	22. Price
unclassified	unclassified	60	A04

NASA FORM 1626 OCT 86

For sale by the National Technical Information Service, Springfield, Virginia 22161-2171

NASA-Langley, 1991